US006032464A

United States Patent [19]

Swift et al.

[11] Patent Number: 6,032,464

[45] Date of Patent: Mar. 7, 2000

[54] **TRAVELING-WAVE DEVICE WITH MASS FLUX SUPPRESSION**

[75] Inventors: **Gregory W. Swift**, Santa Fe; **Scott N. Backhaus**, Los Alamos; **David L. Gardner**, White Rock, all of N.Mex.

[73] Assignee: **Regents of the University of California**, Los Alamos, N.Mex.

[21] Appl. No.: **09/234,236**

[22] Filed: **Jan. 20, 1999**

[51] **Int. Cl.**[7] **F01B 29/10**

[52] **U.S. Cl.** **60/520**; 60/521; 60/522; 62/6

[58] **Field of Search** 60/517, 520, 521, 60/522, 526; 62/6

[56] **References Cited**

U.S. PATENT DOCUMENTS

4,114,380	9/1978	Ceperley	60/721
4,355,517	10/1982	Ceperley	60/721
5,519,999	5/1996	Harpole et al.	60/520 X
5,953,920	9/1999	Swift et al.	60/520 X

OTHER PUBLICATIONS

Peter Hutson Ceperley, "Gain and Efficiency of a Short Traveling Wave Heat Engine," J. Acoust. Soc. Am., vol. 77, No. 3, pp. 1239–1244, Mar. 1985.

Peter Hutson Ceperley, "A Pistonless Stirling Engine—The Traveling Wave Heat Engine," J. Acoust. Soc. Am., vol. 66, No. 5, pp. 1509–1513, Nov. 1979.

Ray Radebaugh, "A Review of Pulse Tube Refrigeration," Adv. In Cryogenic Eng., vol. 35, pp. 1191–1205, New York, 1990.

David Gedeon, "DC Gas Flows in Stirling and Pulse-Tube Cryocoolers," Cryocooler Conference, pp. 1–7, Jun. 1996.

J.R. Olson, G.W. Swift, "Acoustic Streaming in Pulse Tube Refrigerators: Tapered Pulse Tubes," Cryogenics, vol. 37, No. 12, pp. 769–776, 1997.

Primary Examiner—Hoang Nguyen

Attorney, Agent, or Firm—Ray G. Wilson

[57] **ABSTRACT**

A traveling-wave device is provided with the conventional moving pistons eliminated. Acoustic energy circulates in a direction through a fluid within a torus. A side branch may be connected to the torus for transferring acoustic energy into or out of the torus. A regenerator is located in the torus with a first heat exchanger located on a first side of the regenerator downstream of the regenerator relative to the direction of the circulating acoustic energy; and a second heat exchanger located on an upstream side of the regenerator. The improvement is a mass flux suppressor located in the torus to minimize time-averaged mass flux of the fluid. In one embodiment, the device further includes a thermal buffer column in the torus to thermally isolate the heat exchanger that is at the operating temperature of the device.

22 Claims, 16 Drawing Sheets

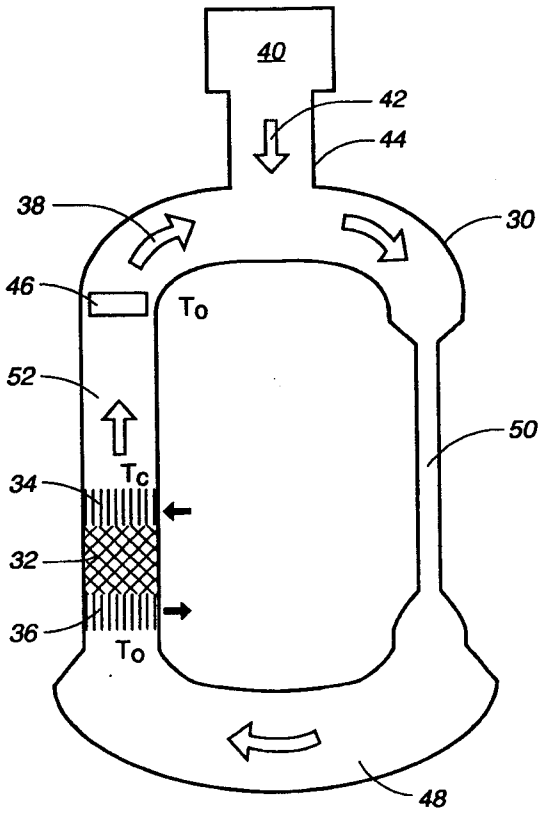

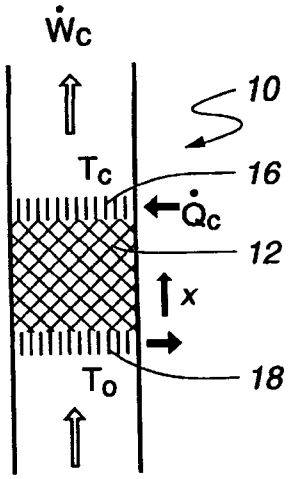

Fig. 1A

(Prior Art Refrigerator)

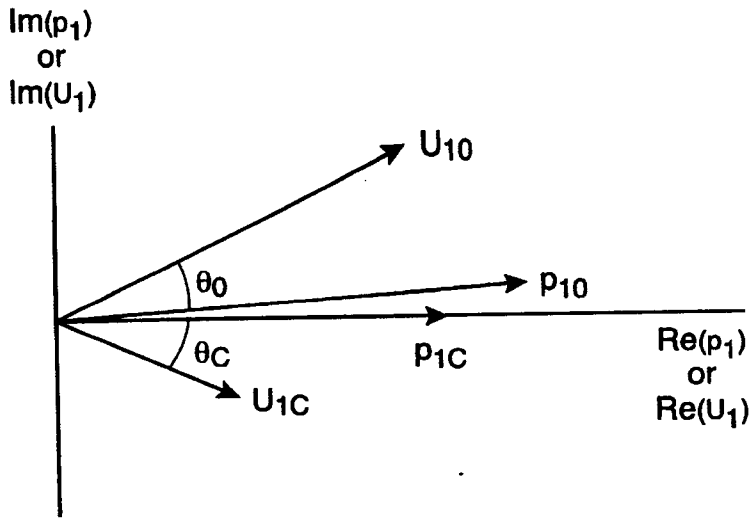

Fig. 1B

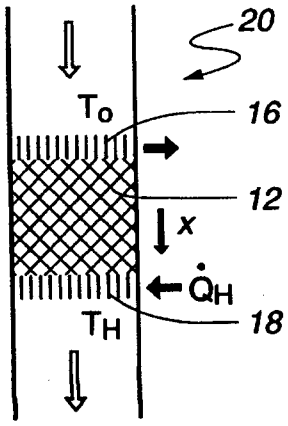

Fig. 2A

(Prior Art Engine)

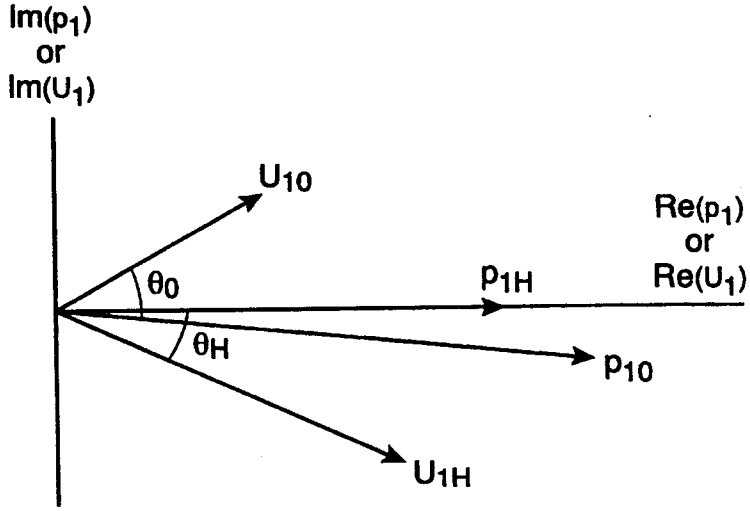

Fig. 2B

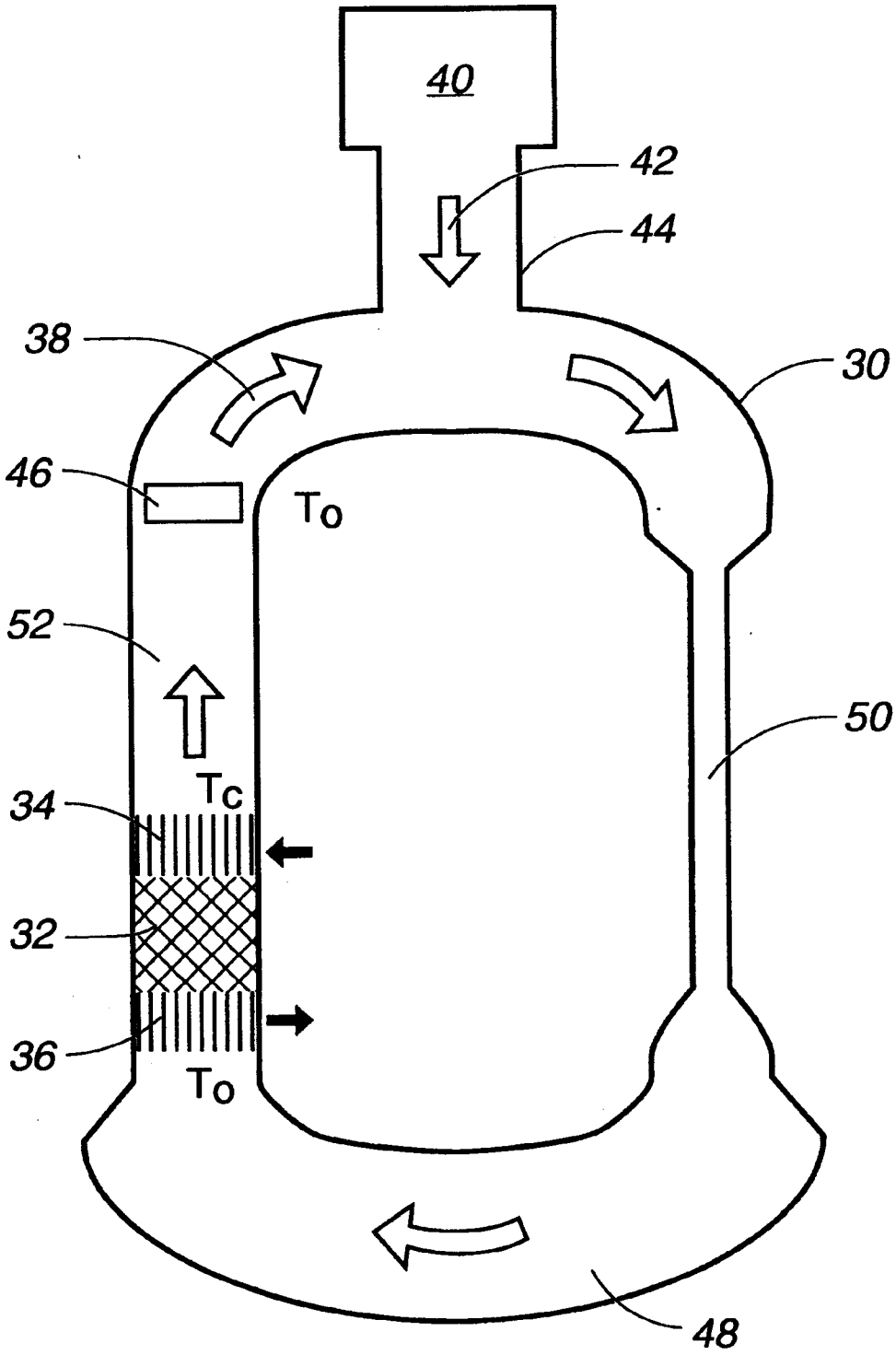

Fig. 3

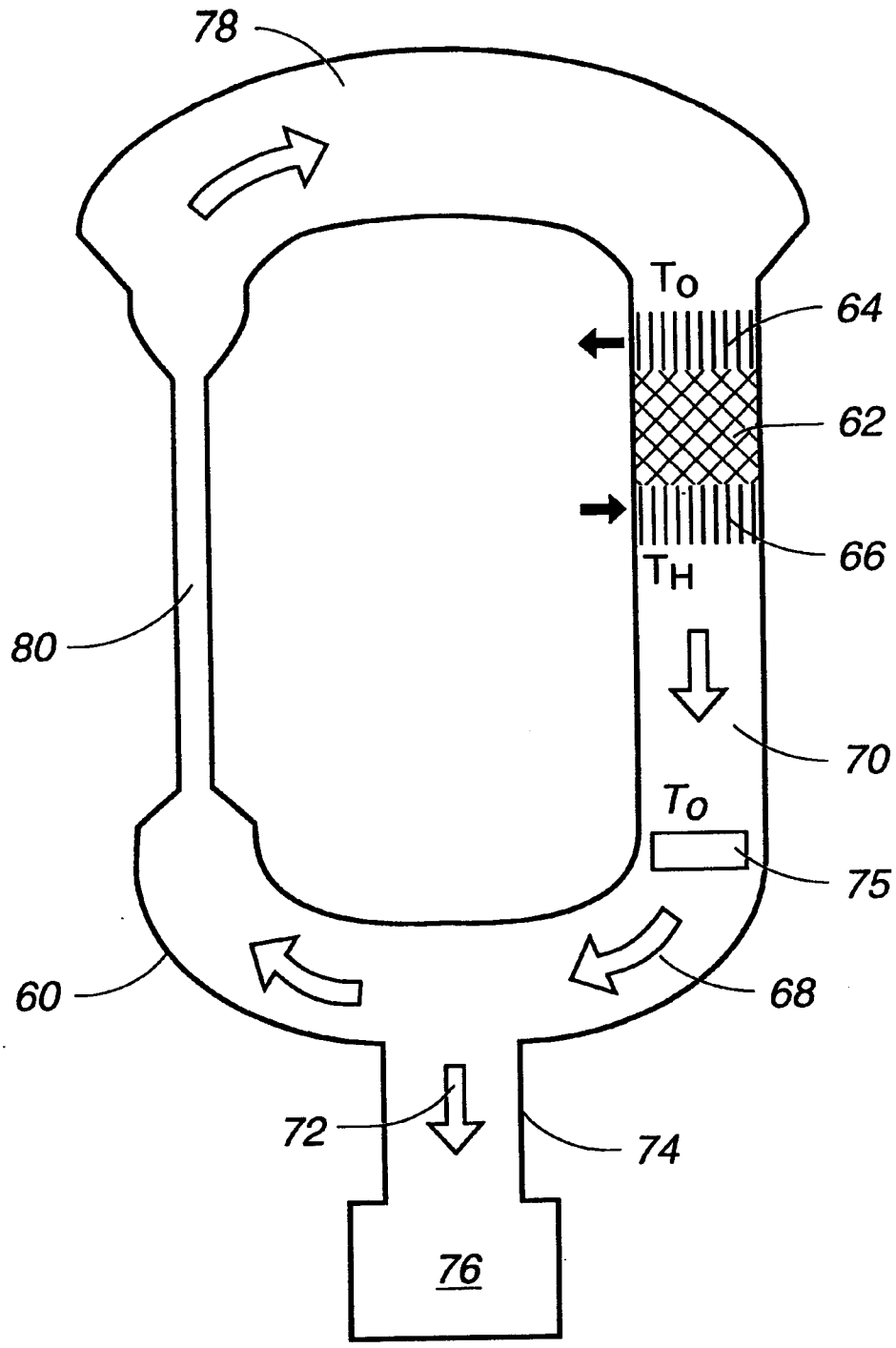

Fig. 4

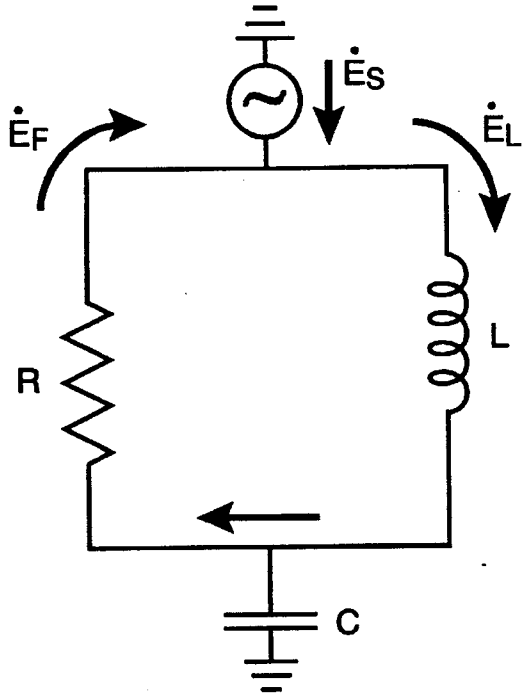

Fig. 5A

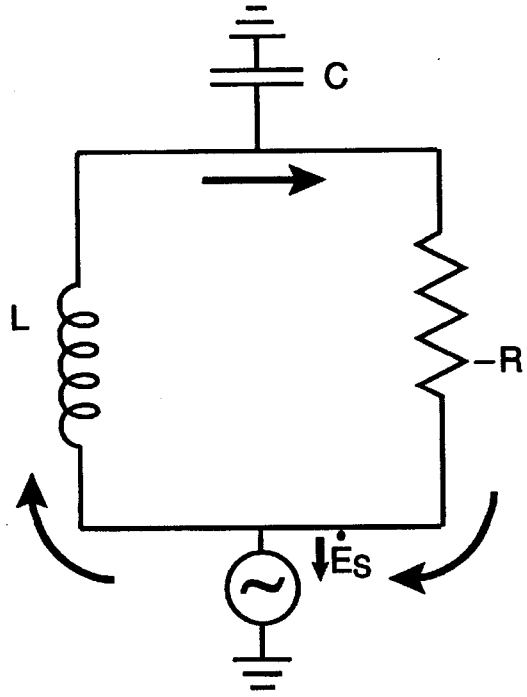

Fig. 5B

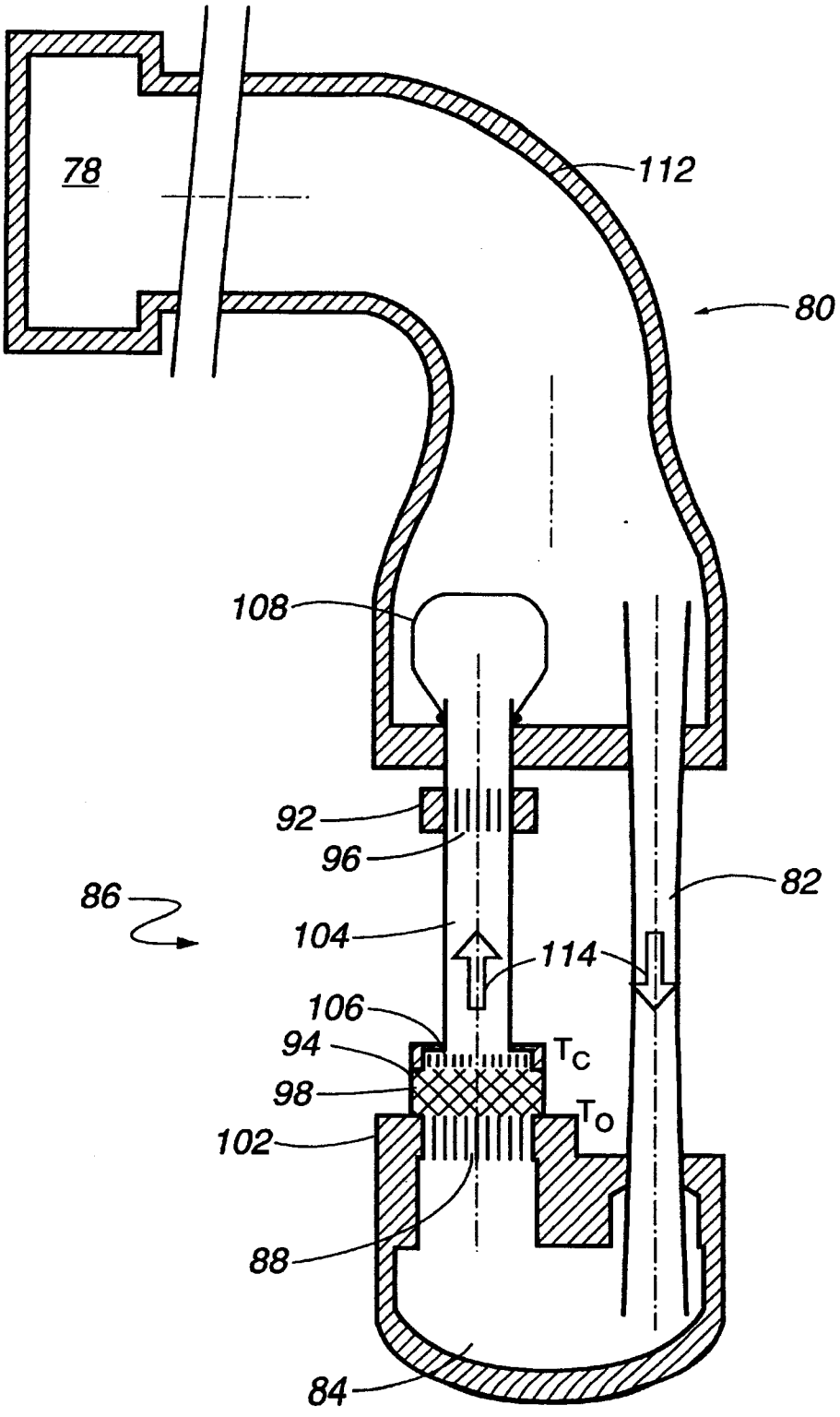

Fig. 6

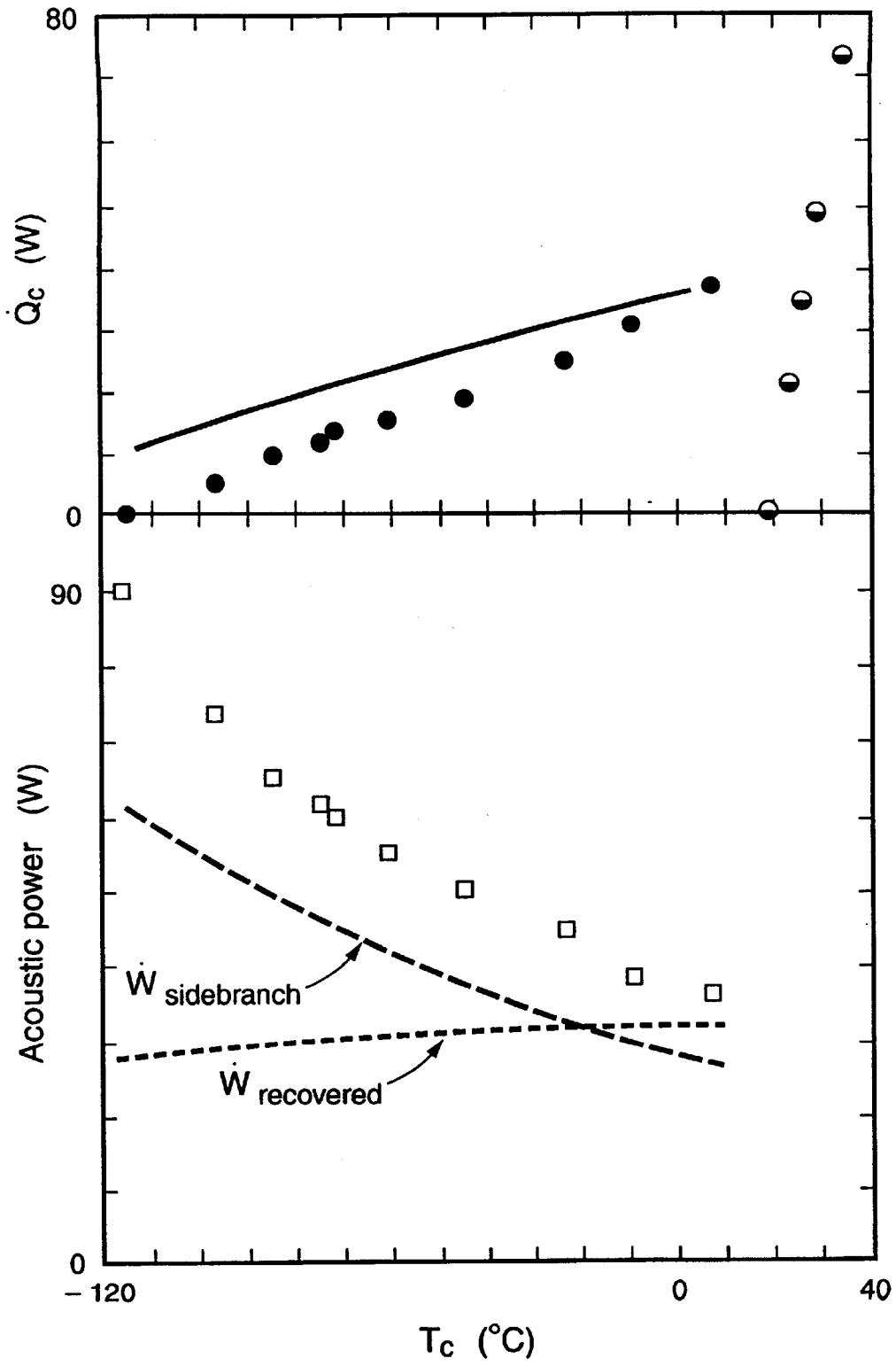
80
$\dot{Q}_c$ (W)
0
90
Acoustic power (W)
$\dot{W}_{sidebranch}$
$\dot{W}_{recovered}$
0
−120
0
40
T_c (°C)

Fig. 7

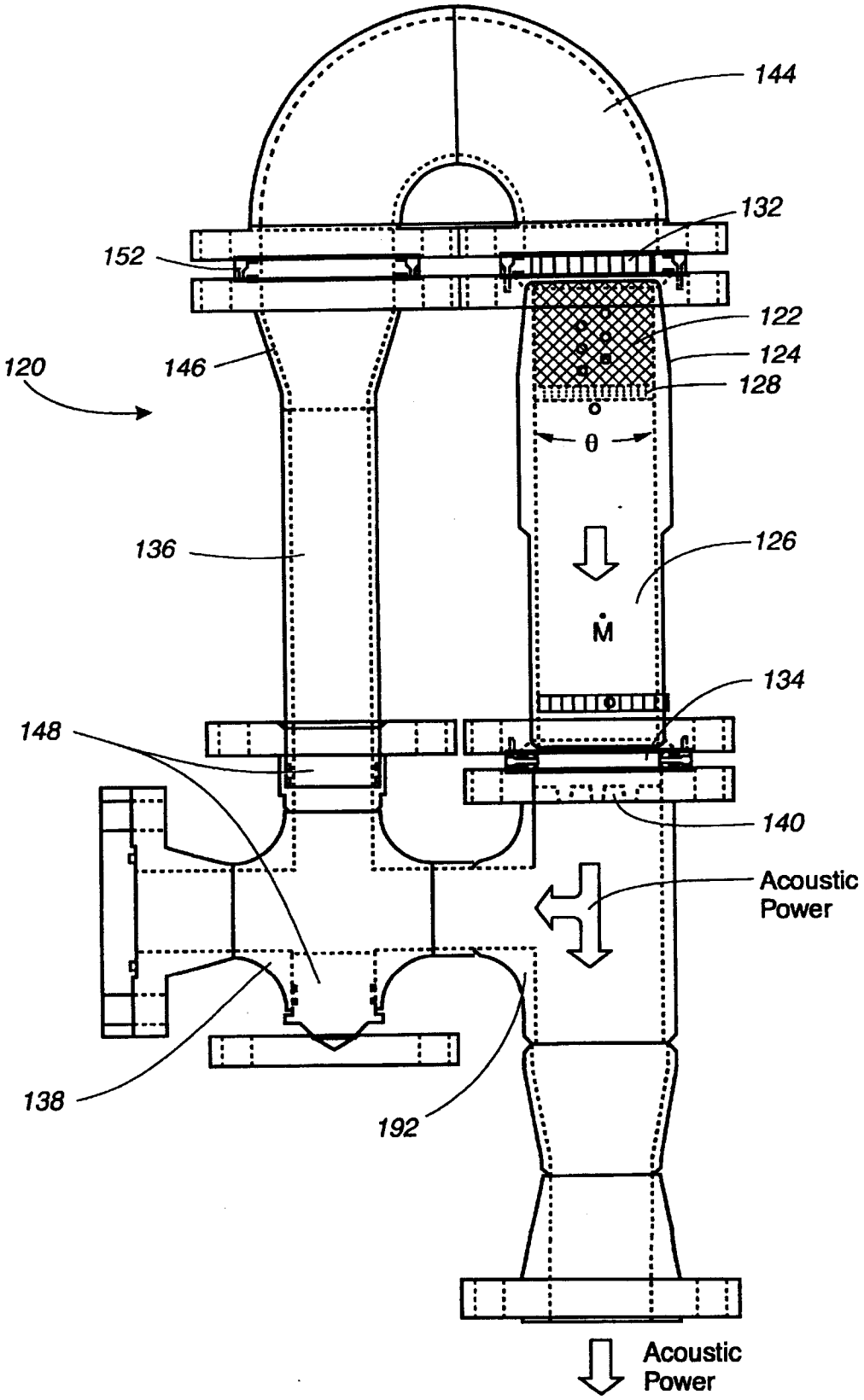
144
132
152
122
124
120
146
128
θ
136
126
M
134
148
140
Acoustic Power
138
192
Acoustic Power

Fig. 8

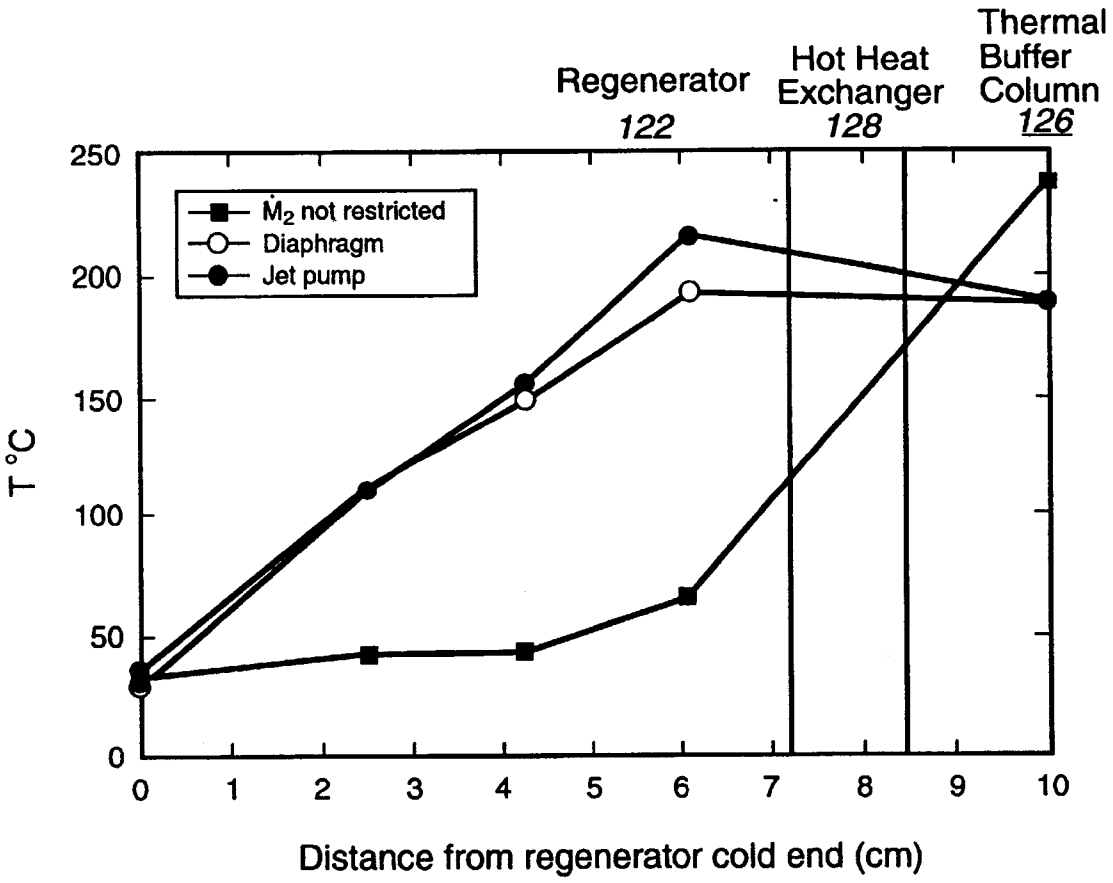
Regenerator
122
Hot Heat
Exchanger
128
Thermal
Buffer
Column
126
250
200
150
100
50
0
T °C
$\dot{M}_2$ not restricted
Diaphragm
Jet pump
0
1
2
3
4
5
6
7
8
9
10
Distance from regenerator cold end (cm)

Fig. 9

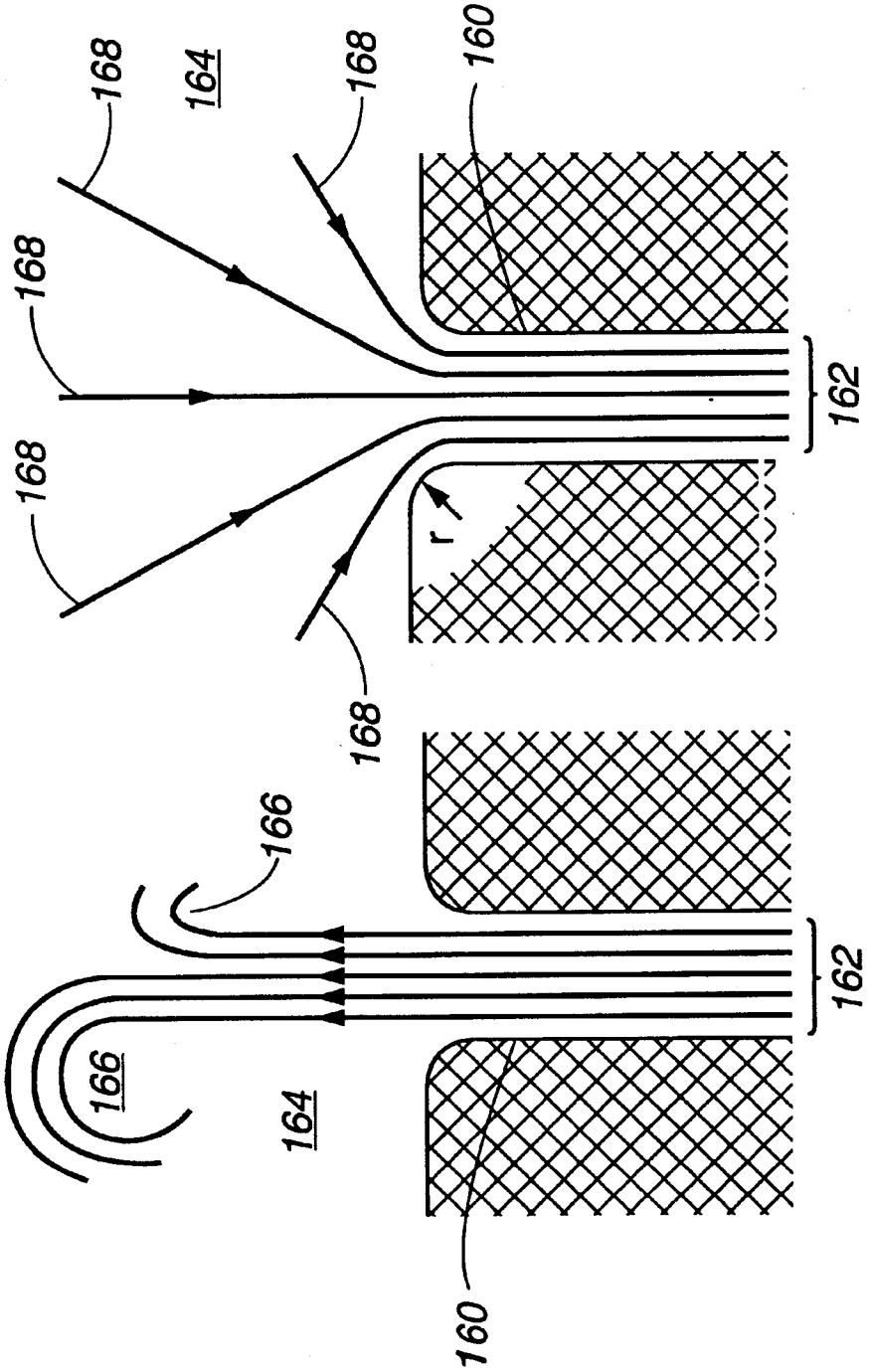

Fig. 10B

Fig. 10A

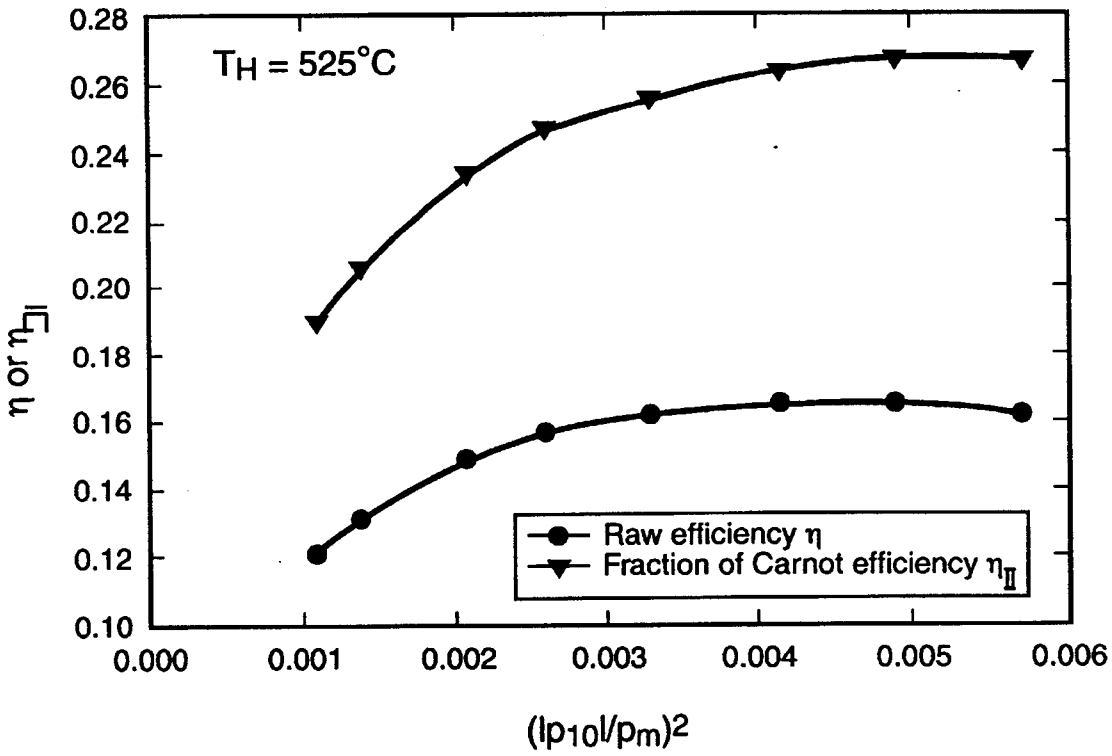
0.28
0.26
0.24
0.22
0.20
0.18
0.16
0.14
0.12
0.10
η or η_II
T_H = 525°C
Raw efficiency η
Fraction of Carnot efficiency η_II
0.000
0.001
0.002
0.003
0.004
0.005
0.006
(|p10|/pm)2

Fig. 11A

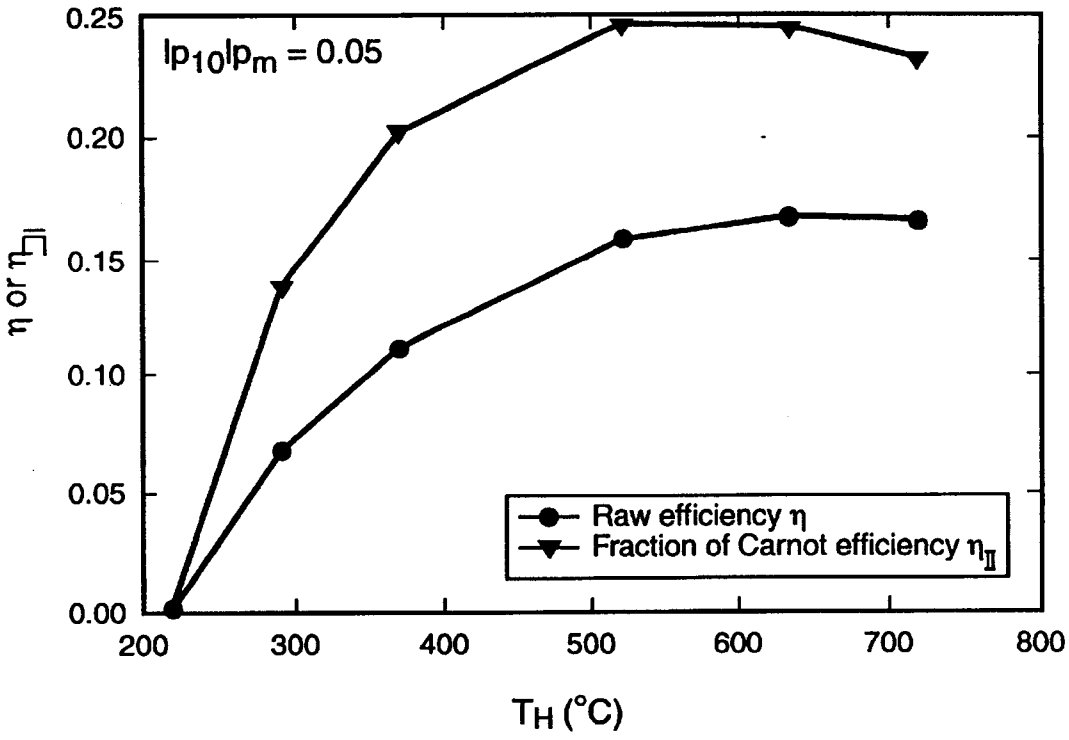
0.25
0.20
0.15
0.10
0.05
0.00
η or η_II
Ip10Ipm = 0.05
Raw efficiency η
Fraction of Carnot efficiency η_II
200
300
400
500
600
700
800
TH (°C)

Fig. 11B

Fig. 12B

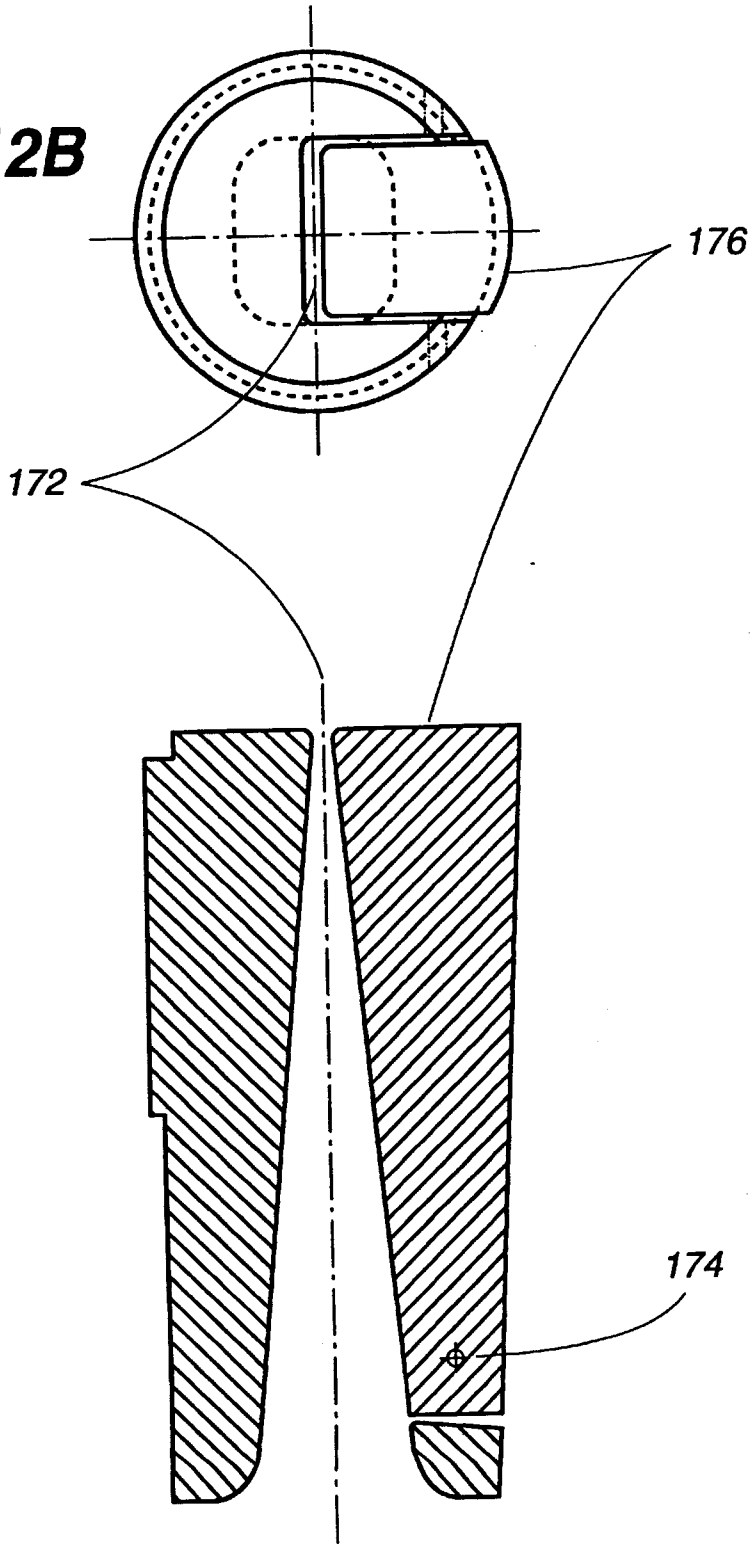

Fig. 12A

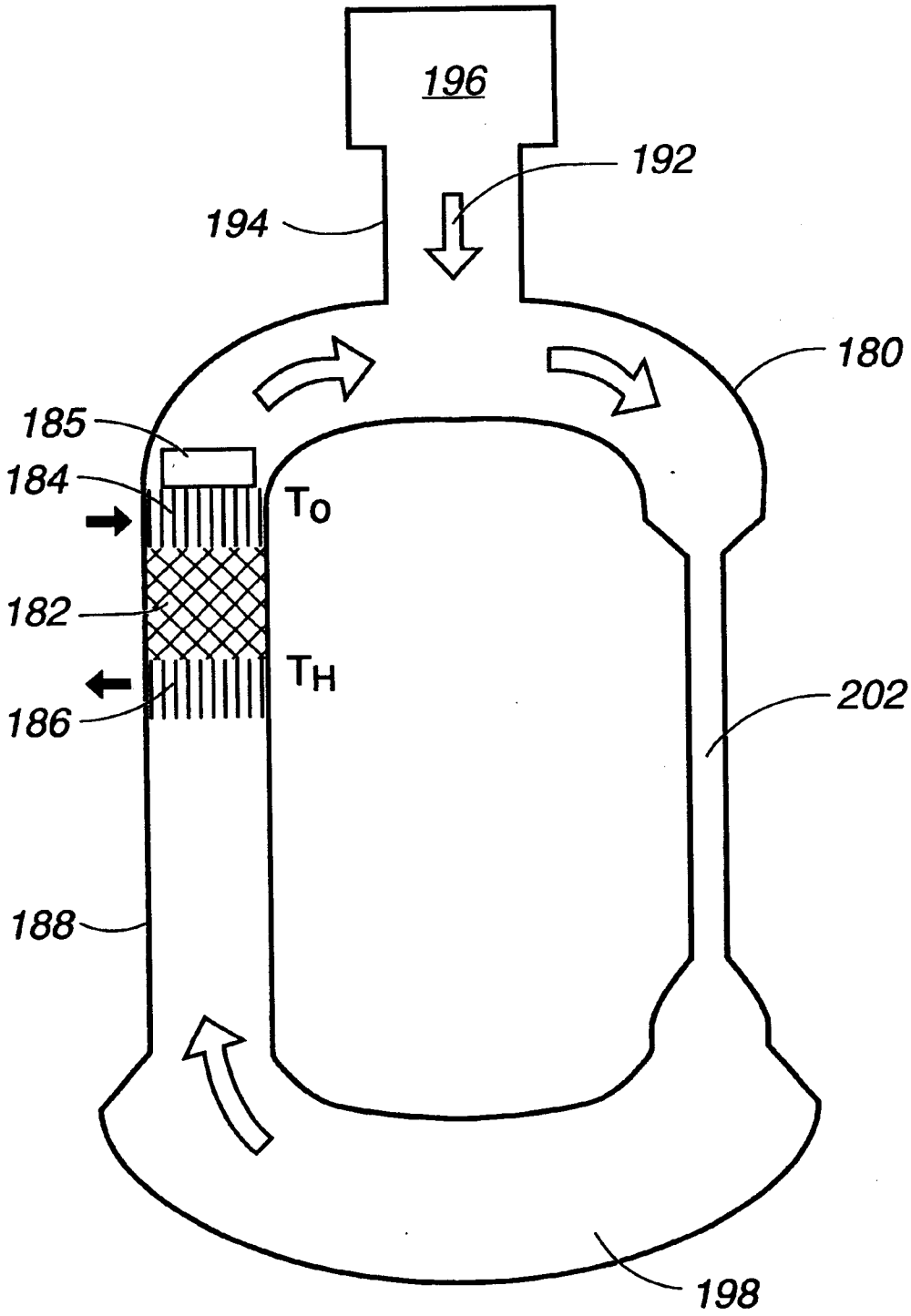

Fig. 13A

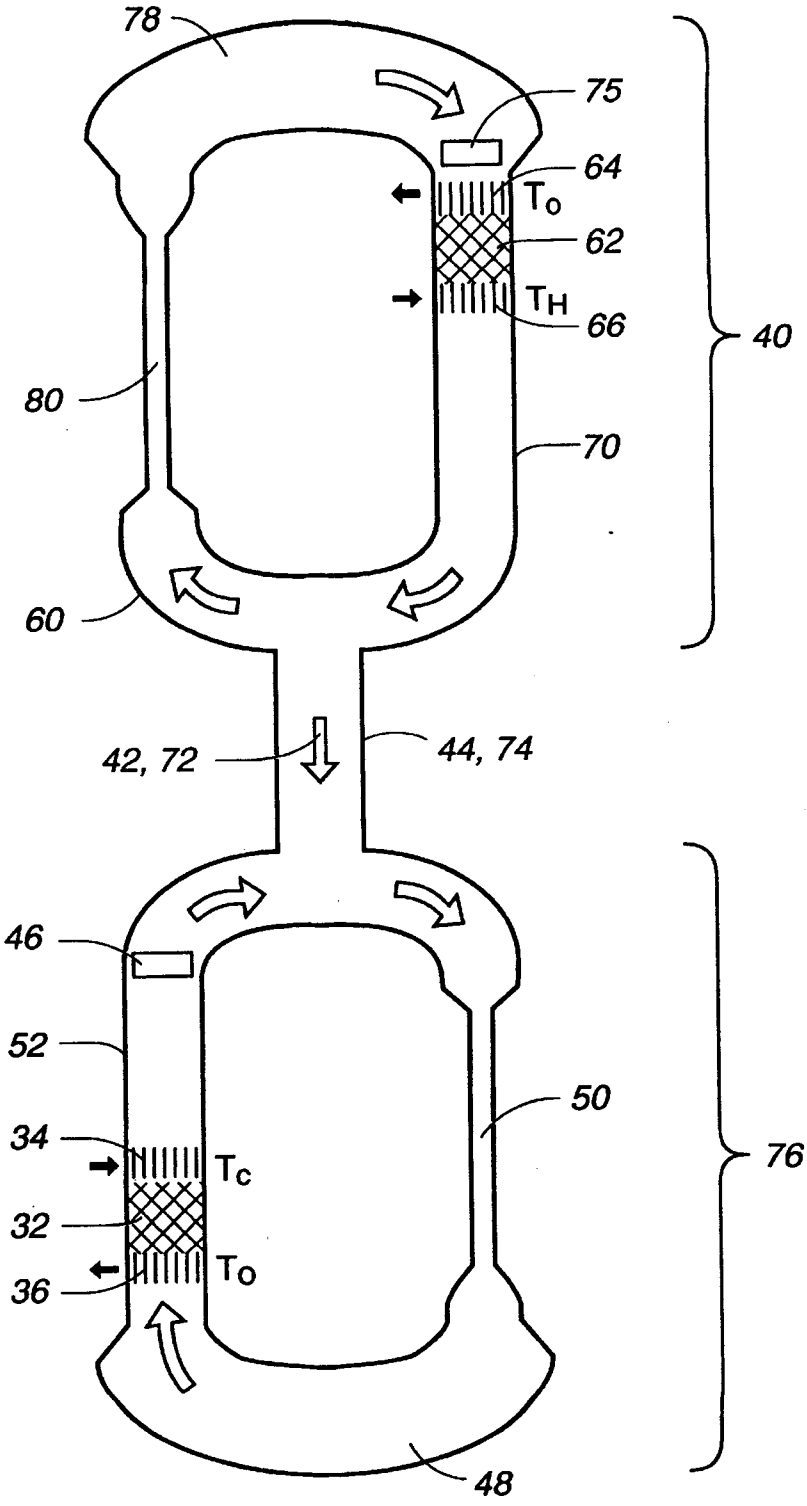
78
75
64
T_O
62
T_H
66
40
80
70
60
42, 72
44, 74
46
52
50
34
T_C
32
T_O
36
76
48

Fig. 13B

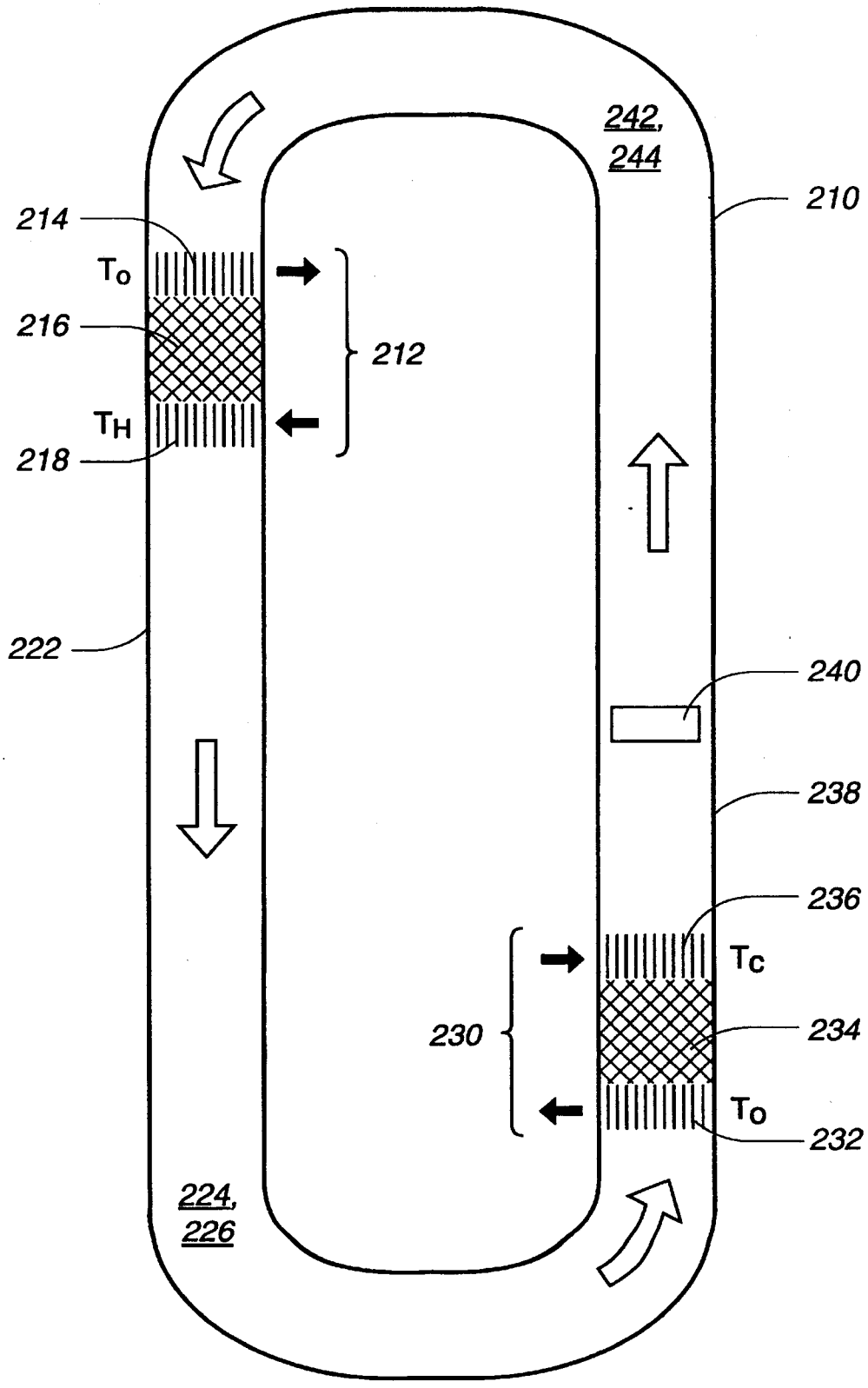
242, 244
210
214
T_O
216
212
T_H
218
222
240
238
236
T_C
230
234
T_O
232
224, 226

Fig. 13C

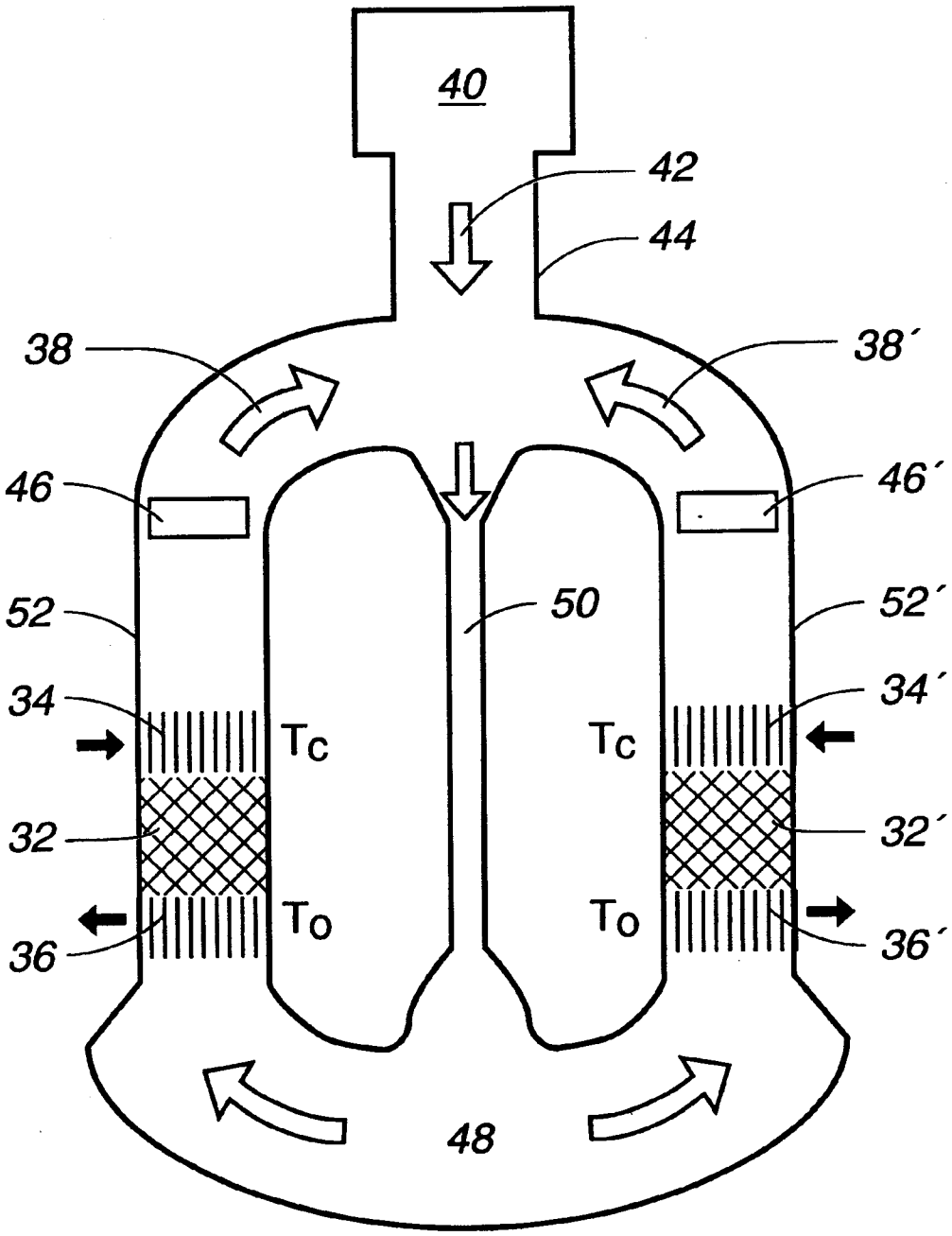

Fig. 13D

TRAVELING-WAVE DEVICE WITH MASS FLUX SUPPRESSION

STATEMENT REGARDING FEDERAL RIGHTS

This invention was made with government support under Contract No. W-7405-ENG-36 awarded by the U.S. Department of Energy. The government has certain rights in the invention.

FIELD OF THE INVENTION

The present invention relates generally to traveling-wave engines and refrigerators, and, more particularly, to traveling-wave engines and refrigerators that perform as Stirling engines and refrigerators.

BACKGROUND OF THE INVENTION

There are a number of important antecedents to this invention. The most important antecedents are Stirling engines and refrigerators, a century old. An important step in the elimination of moving parts from Stirling engines and refrigerators came in 1969, when William Beale invented the "free-piston" variety of Stirling devices, in which the crankshaft and linkages were replaced by gas springs, so that gas spring constants and piston masses could be chosen to cause resonant motion of the pistons with the desired frequency, amplitudes, and phases.

Ceperley, "Gain and efficiency of a short traveling-wave heat engine," 77 *J. Acoust Soc. Am.*, pp. 1239–1294 (1985) suggested that the essence of Stirling engines and refrigerators is a regenerator (and adjacent heat exchangers) in which the pressure and velocity oscillations are substantially in phase, reminiscent of an acoustic traveling-wave, and hence that an acoustic network with essentially toroidal topology containing the Stirling heat-exchange components can provide such phasing. Ceperley claimed that efficiencies near 80% of the Carnot efficiency are in principle possible with such configurations. Ceperley's contribution could be seen as an extension of Beale's, in that Ceperley uses gas inertia effects in addition to Beale's gas spring effects, thereby eliminating the massive pistons of Beale's invention. Other related teachings by Ceperley are set out in U.S. Pat. No. 4,113,380, issued Sep. 19, 1978, and U.S. Pat. No. 4,355,517, issued Oct. 26, 1982. However, Ceperley presented no teachings on how to realize a practical device.

The conventional orifice pulse tube refrigerator (OPTR) (Radebaugh, "A review of pulse tube refrigeration," 35 Adv. *Cryogenic Eng.*, pp. 843–844 (1992)) operates thermodynamically like a Stirling refrigerator, but with the cold moving parts replaced by passive components: a thermal buffer column known as the pulse tube, and a dissipative acoustic impedance network. The efficiency $\dot{Q}_C/\dot{W}$ of an OPTR is fundamentally limited by the temperature ratio T_C/T_0, which is lower than the Carnot value $T_C/(T_0-T_C)$ because of the inherent irreversibility in the dissipative acoustic impedance network. T is temperature, $\dot{Q}_C$ is heat, $\dot{W}$ is work, and the subscripts **0**, and C refer to ambient and cold, respectively. The OPTR can be regarded as another means to eliminate moving parts from Stirling devices. However, the efficiency of an OPTR is fundamentally less than that of a Stirling device, and the OPTR is only applicable to refrigerators.

Conventional OPTRs have long used the thermal buffer column known as a pulse tube, but until recently this component carried substantial heat leak. However, using a tapered tube, as described in U.S. patent application Ser. No.

08/975,766, filed Nov. 21, 1997, can reduce the heat leak along such a thermal buffer column to as little as 5% of the cooling power of a OPTR. Thermal buffer columns have been used in two-piston Stirling refrigerators as well as in OPTRs, but not in Stirling engines.

In the context of double-inlet OPTRs, Gedeon, "DC gas flows in Stirling and pulse-tube cryocoolers," in Ross ed., *Cryocoolers* 9, pp. 385–392 (Plenum, N.Y. 1997) discusses how nonzero time-averaged mass flux $\dot{M}$ can arise in Stirling and pulse-tube cryocoolers whenever a closed-loop path exists for steady mass flux. It is essential that $\dot{M}$ through a Stirling engine or refrigerator be near zero, to prevent a large steady energy flux $\dot{M}c_p(T_0-T_C)$ from adding an unwanted thermal load to the cold heat exchanger of a refrigerator, or to prevent a large steady energy flux $\dot{M}c_p(T_H-T_0)$ from removing a large amount of heat from the hot heat exchanger of an engine—in either case, reducing the efficiency. Here c_p is the gas isobaric specific heat per unit mass.

Another, less directly related antecedent to this invention is the set of prior thermoacoustic engines and refrigerators developed in the past 20 years at Los Alamos National Laboratory and elsewhere. These operate on an intrinsically irreversible cycle, using nearly standing-wave phasing between gas pressure oscillations and velocity oscillations and using deliberately imperfect thermal contact in the stack (which might otherwise be mistaken for a regenerator). The intrinsic irreversibility and other practical issues have thus far limited the best standing-wave thermoacoustic engines and refrigerators to below 25% of the Carnot efficiency.

Various objects, advantages and novel features of the invention will be set forth in part in the description which follows, and in part will become apparent to those skilled in the art upon examination of the following or may be learned by practice of the invention. The objects and advantages of the invention may be realized and attained by means of the instrumentalities and combinations particularly pointed out in the appended claims.

SUMMARY OF THE INVENTION

To achieve the foregoing and other objects, and in accordance with the purposes of the present invention, as embodied and broadly described herein, the present invention includes a pistonless Stirling device. Acoustic energy circulates in a direction through a fluid within a torus. In one embodiment, a side branch is connected to the torus for transferring acoustic energy into or out of the torus. A regenerator is located in the torus with a first heat exchanger located on a first side of the regenerator downstream of the regenerator relative to the direction of the circulating acoustic energy; and a second heat exchanger located on a second side of the regenerator, where one of the heat exchangers is at an operating temperature and the other one of the heat exchangers is at ambient temperature. The improvement herein comprises a mass flux suppressor located in the torus to minimize time averaged mass flux of the fluid. In one embodiment, the device further includes a thermal buffer column adjacent to the heat exchanger at the operating temperature to thermally isolate the heat exchanger at the operating temperature.

BRIEF DESCRIPTION OF THE DRAWINGS

The accompanying drawings, which are incorporated in and form a part of the specification, illustrate embodiments of the present invention and, together with the description, serve to explain the principles of the invention. In the drawings:

FIGS. 1A and 1B schematically depict the heat-exchange components of a prior art Stirling-cycle refrigerator and accompanying phasor diagram, respectively.

FIGS. 2A and 2B schematically depict the heat-exchange components of a prior art Stirling-cycle engine and accompanying phasor diagram.

FIG. 3 schematically depicts one embodiment of a Stirling-cycle refrigerator according to the present invention.

FIG. 4 schematically depicts one embodiment of a Stirling-cycle engine according to the present invention.

FIGS. 5A and 5B depict electrical circuit analogues for basic aspects of the present invention.

FIG. 6 is a cross-sectional view of a refrigerator version of the present invention with a diaphragm mass flux suppressor.

FIG. 7 graphically depicts the power flows as a function of the cold heat exchanger temperature T_C for the refrigerator shown in FIG. 6.

FIG. 8 is a cross-sectional view of an engine version of the present invention with a hydrodynamic mass flux suppressor.

FIG. 9 graphically depicts temperature profiles within the regenerator of the engine shown in FIG. 8.

FIGS. 10A and 10B schematically illustrate asymmetric mass flux through a hydrodynamic mass flux suppressor.

FIG. 11A graphically depicts the efficiencies of the engine shown in FIG. 8 at T_H=525° C.

FIG. 11B graphically depicts the efficiencies of the engine shown in FIG. 8 with $|p_1|/p_m$=0.05

FIGS. 12A and 12B are a cross-sectional side view and a top view, respectively, of a variable slit mass flux suppressor for use in the present invention.

FIG. 13A schematically depicts a heat pump adaptation of the refrigerator shown in FIG. 3.

FIG. 13B schematically depicts the refrigerator shown in FIG. 3 driven by the engine shown in FIG. 4.

FIG. 13C schematically depicts a heat-driven refrigerator located in a single torus.

FIG. 13D schematically depicts a plurality of refrigerators shown in FIG. 3 connected in parallel and driven from a single source.

DETAILED DESCRIPTION

In accordance with the present invention, a new class of engines and refrigerators operate thermodynamically like Stirling engines and refrigerators, but all moving parts are eliminated by using acoustic phenomena in place of the pistons that have previously been used in Stirling devices. Thus, both the efficiency advantage of the Stirling cycle (whose inherent limit is the Carnot efficiency) and the no-moving-parts simplicity/reliability advantage of intrinsically irreversible thermoacoustics are obtained in these devices.

The essential components of a Stirling refrigerator **10** and a Stirling engine **20**, shown in FIGS. 1A and 2A, are regenerators **12**, each with two adjacent heat exchangers **16**, **18**. A gas (or other thermodynamically active fluid) is made to experience pressure oscillations and displacement oscillations throughout these components, with phasing such that acoustic power enters the components at the ambient-temperature end T_0 and leaves at the other end at cold temperature T_C, or hot temperature T_H, as shown by the long broad arrows in FIGS. 1A and 2A. Regenerators **12** have heat capacity, and the gas passages within regenerators **12** have hydraulic radii smaller than the thermal penetration depth in the gas.

To consider the thermodynamic cycle quantitatively, assume the essential physics to be spatially one dimensional, with x specifying the coordinate along the direction of oscillatory gas motion. Conventional counterclockwise phasor notation is used, so that time-dependent variables are expressed as

$$\xi(x,t)=\xi_m(x)+Re[\xi_1(x)e^{i\omega t}] \quad (1)$$

with the mean value ξ_m real and independent of time t, and with $\xi_1(x)$ complex to account for both the magnitude and phase of the oscillation, which occurs at angular frequency $\omega=2\pi f$, where f is the ordinary frequency. An acoustical point of view is presented, using the vocabulary of acoustic resistance, inertance, compliance, and transmission line to discuss the lumped and distributed impedances associated with the components of the engine or refrigerator. This approach has been successful previously, even within regenerators (see, e.g., Swift et al., "Simple harmonic analysis of regenerators," **10** *Journal of Thermophysics and Heat Transfer,* pp. 652–662 (1996)). The present approach focuses primarily on conventional acoustic variables: pressure amplitude p_1 and volumetric velocity U_1. The positive direction for x and U_1 is taken as the direction of positive acoustic power flow.

Features of phasor diagrams for efficient Stirling engines and refrigerators are shown in FIGS. 1B and 2B. The capitalized subscripts on variable such as p_1 and U_1 correspond to the locations labeled with T having the same subscripts in FIGS. 1A and 2A and subsequent Figures. The arbitrary convention is adopted that the phases of the pressure at the refrigerator's cold heat exchanger (e.g., heat exchanger **16**, FIG. 1A) and the engine's hot heat exchanger (e.g., heat exchanger **18**, FIG. 1A) are zero, so p_{1C} in FIG. 1B and p_{1H} in FIG. 2B fall on the real axis. Typically the pressure drop across the heat exchangers is negligible compared to that across the regenerator, which is in turn small compared to $|p_1|$, so p_{10} must lie close to p_{1C} or p_{1H}, as shown in FIGS. 1B and 2B.

Typically the time-averaged energy flux through the regenerator is small. Applying energy conservation to cold heat exchanger **16** in FIG. 1A then shows that the cooling power $\dot{Q}_C$, shown by the short heavy arrow, is about equal to the total acoustic power flowing out of the cold heat exchanger in the positive x direction, $\dot{W}_C=\frac{1}{2}Re[p_{1C}\tilde{U}_{1C}]=\frac{1}{2}|p_{1C}||U_{1C}|\cos\theta_C$, shown by the long arrow in FIG. 1A, where θ_C is the phase angle between p_{1C} and U_{1C}. In fact, heat leaks can flow to the cold heat exchanger, so the acoustic power is an upper bound on the actual cooling power:

$$\dot{Q}_C \leqq \frac{1}{2}Re[p_{1C}\tilde{U}_{1C}] \quad (2)$$

In FIG. 1A, in order to achieve positive cooling power, acoustic power must flow in the direction shown with the long arrows, in the positive x direction, so U_{10} and U_{1C} must lie in the right half plane in FIG. 1B. An idealized regenerator might be imagined with negligible entrained gas volume, so that $\rho_m U_1$ U would be independent of x in the regenerator (where ρ_m is the gas mean density), and in particular the phase of U_1 would be constant throughout the regenerator. However, it is well known that nonzero gas volume in the regenerator causes x dependence in U_1 proportional to the local gas volume and to $i\omega p_1$. This leads to a spread in phase of U_1 through the system, with U_1 at

small x (i.e. toward ambient heat exchanger **18**) leading. The most efficient regenerator operation occurs when $|U_1|$ is as small as possible for a given cooling power, because this leads to minimal viscous pressure drop across the regenerator and minimal energy flux through the regenerator due to imperfect thermal contact in the regenerator. To achieve small $|U_1|$ for a given $\dot{W}_C$, U_1 should be nearly in phase with p_1, so the phase of p_1 should fall somewhere between the phases of U_{1C} and U_{10}. Viscous pressure drop occurs throughout the regenerator, so $p_{10}-p_{1C}$ must be in phase with (parallel to) some weighted average of U_1 in the regenerator. Both $|U_1|$ and viscosity are highest at the regenerator's ambient end T_0, so the weighted average is typically dominated by U_{10}, usually ensuring that p_{10} leads p_{1C}. All these features are illustrated in FIG. **1B**.

Much of the above discussion also applies directly to an engine. As noted above, the components of a Stirling engine, shown in FIG. **2A**, are nearly identical to those of a Stirling refrigerator. The main difference is that regenerator **12** in the engine produces work while the refrigerator's regenerator **12** absorbs work. This difference can be seen in the phasor diagram of FIG. **2B**. With $\theta_0<90°$, acoustic power flows into the ambient side of regenerator **12**. The mean temperature $T_m(x)$ rises from T_O to T_H through regenerator **12**. This increase in T_m causes ρ_m to fall. Since the first-order mass flux $\rho_m U_1$ is nearly independent of x, the volume velocity increases, so $|U_{1H}|>|U_{10}|$. In addition, the volume of gas entrained in the regenerator causes the phase of U_1 to rotate in a similar fashion as in the refrigerator. These two effects locate U_{1H} relative to U_{10} in FIG. **2B**. The amplification of the acoustic power is indicated by

$$\tfrac{1}{2}|p_{1H}||U_{1H}|\cos\theta_H>\tfrac{1}{2}|p_{10}||U_{10}|\cos\theta_0.$$

Since the time-averaged energy flux through regenerator **12** is small, the acoustic power flowing out of hot heat exchanger **18** is nearly equal to the heat flowing into hot heat exchanger **18**. Again, heat leaks and other losses reduce this power making Q_H an upper bound on the acoustic power, i.e., $\tfrac{1}{2}\mathrm{Re}(p_{1H}\tilde{U}_{1H})\leqq\dot{Q}_H$. The location of p_{10} relative to p_{1H} is due to viscous pressure drop within regenerator **12**, with the difference $p_{10}-p_{1H}$ proportional to a weighted average of U_1 through regenerator **12**. Similar to the refrigerator, the viscous effects are largest at the hot end of regenerator **12**, where $|U_1|$ is largest and viscosity is largest. Hence, with U_{1H} dominating, p_{10} lags p_{1H} slightly.

Returning now to the refrigerator, as discussed above, the acoustic power

$$\dot{W}_C=\frac{\omega}{2\pi}\int_0^{2\pi/\omega}p(t)U(t)dt=\frac{1}{2}Re[p_{1C}\tilde{U}_{1C}] \tag{3}$$

flows out of the refrigerator's **10** cold heat exchanger **16**. As taught by Ceperley, ideally this acoustic power should be transmitted without loss to the ambient heat exchanger. To accomplish this, Ceperley prescribed a full-wavelength torus transmitting the acoustic wave. But, in accordance with one aspect of the present invention, it is advantageous to use a much shorter sub-wavelength torus **30**, shown schematically in FIG. **3**, because it is more compact.

FIG. **3** shows an embodiment of a refrigerator version of the present invention. A torus **30** with total length less than a quarter of the acoustic wavelength contains the Stirling refrigerator regenerator **32** and two heat exchangers **34**, **36**. As used herein, the term "torus" means a pipe, tube, or the like that defines a circulation path that is a loop that is circular or elongated, having a cross-section for supporting an acoustic wave, preferably circular. Acoustic power **38** circulates clockwise around torus **30**, as shown by the long arrows. Additional acoustic power **42** generated by acoustic device **40** (such as an intrinsically irreversible thermoacoustic engine, a loudspeaker, a motor-driven piston, or a traveling-wave engine) enters torus **30** from side branch **44**, to make up for acoustic power lost in regenerator **32** and elsewhere in the torus. As more fully explained below, a mass flux suppressor **46** is located within torus **30** to reduce the time-averaged mass flux $\dot{M}$ substantially to zero.

In one embodiment, the flow resistance of mass flux suppressor **46**, shown in FIG. **3**, has a resistance R_M such that

$$p_{1C}-p_{1J}=R_M U_{1M}, \tag{4}$$

where subscript J signifies the location of the junction between torus **30** and side branch **44**. A compliance portion **48** of torus **30** ensures that the volumetric velocity U_{1L} through an inertance portion **50** of torus **30** differs from that through ambient heat exchanger **36**:

$$U_{1L}=U_{10}+j\frac{\omega V_0}{\gamma p_m}p_{10} \tag{5}$$

where V_0 is the volume of the compliance portion **48** of torus **30**, so that the pressure difference across inertance **50** is

$$p_{1J}-p_{10}=j\omega\frac{\rho_m l}{S}\left(U_{10}+j\frac{\omega V_0}{\gamma p_m}p_{10}\right) \tag{6}$$

where l and S are the length and area, respectively, of inertance **50**. Taking the phasors at C, M, and **0** to be given and combining Equations (4) and (6) to eliminate p_{1J}, a single complex equation is obtained in the unknowns R_M, V_0, l, and S, generally with many possible solutions that enable a refrigerator to be built according to the present invention.

An embodiment of the engine version of the invention is shown schematically in FIG. **4**. Torus **60**, whose total length is less than a quarter wavelength, contains the Stirling engine's regenerator **62** and heat exchangers **64**, **66**. As shown by the long arrows **68**, acoustic power circulates clockwise around torus **60**. Surplus acoustic power **72** generated by the engine may be tapped off by side branch **74**, and is available to perform useful work through acoustic device **76** (which could be a piezoelectric or electrodynamic transducer, an orifice pulse tube refrigerator, or a refrigerator according to the present invention). Acoustic power **68** circulates around the torus and provides the input work to the ambient end T_0 of the Stirling engine. Therefore, this circulating work **68** replaces the ambient piston in a conventional Stirling engine. Mass-flux suppressor **75** again acts to reduce the time-averaged mass flux $\dot{M}$ toward zero. The analysis of short torus **60** is entirely parallel to Equations (4)–(6), and follows by merely replacing the subscript C with H.

The choice of an operating frequency for the devices shown in FIGS. **3** and **4** involves a compromise among many issues. High frequency leads to high power per unit volume of the device, because many thermodynamic cycles are performed per unit time and because lengths of the device along propagation direction x scale approximately with wavelength, which is inversely proportional to frequency. On the other hand, low frequency eases the design and

construction of heat exchangers and regenerators, whose pore sizes scale approximately with thermal penetration depth, which is inversely proportional to the square root of the frequency.

The fact that acoustic power will naturally circulate clockwise around the tori of FIGS. **3** and **4**, even though the tori are shorter than a quarter of an acoustic wavelength in exemplary embodiments, seems surprising. But consider the electrical circuits of FIGS. **5A** and **5B**, containing a resistance R, an inductance L, and a capacitance C, crudely analogous to the acoustic circuits of FIGS. **3** and **4**, respectively. Resistance R is crudely analogous to the regenerator and heat exchangers, inductance L is analogous to the acoustic inertance, and capacitance C is analogous to the acoustic compliance.

Derivation of expressions for the ac currents in each component of the electrical circuits is straightforward, and allows further derivation of expressions for the electric power $\dot{E}$ flowing at each location in the circuit. In these idealized circuits, no time-averaged power can be absorbed in the dissipationless inductor L nor flow into the dissipationless capacitor C. Ordinary ac circuit analysis easily yields the fed-back power

$$\dot{E}_F = \frac{1}{2} Re\left[V_{1S}\tilde{I}_{1R}\right] = \frac{|V_{1S}|^2}{2R}\omega^2 L \frac{C(1-\omega^2 LC)}{(1-\omega^2 LC)+(\omega L/R)^2} \quad (7)$$

in FIG. **5A**, with the sign convention as shown in the figure. Hence, whenever $\omega^2 LC<1$ the directions of time-averaged power flow are as shown by the arrows in FIG. **5A**; with positive electric power flowing clockwise around the circuit, analogous to the clockwise circulation of acoustic power in FIG. **3**. By energy conservation, the time-averaged power $\dot{E}_L-\dot{E}_F$ dissipated in the resistor must equal the time-averaged power $\dot{E}_S=\frac{1}{2}Re|V_{1S}\tilde{I}_{1S}|$ flowing from the voltage source into the circuit. If the resistance R is negative, as shown in FIG. **5B**, power also circulates in the clockwise direction and the time-averaged power created in the negative resistance flows out of the circuit and into the voltage source.

It will be apparent to those skilled in the art of acoustics that inertances **50, 80** in FIGS. **3** and **4** may include significant compliance, and that compliances **48, 78** in FIGS. **3** and **4** may include significant inertance. In fact, the function of these components may be served equally well by a short acoustic transmission line having distributed inertances and compliances throughout. For ease of discussion herein, the inertance and compliance are considered as lumped components.

In the refrigerator of FIG. **3**, it is desirable to eliminate heat leaks from ambient to cold heat exchanger **34** in order to have the greatest possible cooling power. Similarly, in the engine of FIG. **4** it is desirable to eliminate heat leaks from hot heat exchanger **66** to ambient in order to minimize the heater power required to run the engine. Regenerators **32, 62** provide this thermal isolation on one side of cold heat exchanger **34** (in a refrigerator) or hot heat exchanger **66** (in an engine) in the present invention, as in all prior Stirling devices. On the other side of heat exchangers **34, 66**, in accordance with one aspect of the present invention, thermal buffer columns **52, 70**, as shown in FIGS. **3** and **4**, eliminate heat leaks. The gas in the thermal buffer columns **52, 70** can be thought of as an insulating piston, transmitting pressure and velocity from the cold **34** or hot **66** heat exchangers to ambient temperatures. The thermal buffer columns **52, 70** are exactly analogous to the pulse tube of an orifice pulse tube refrigerator. Convective heat transfer of various forms could carry heat through thermal buffer columns **52, 70** between the cold **34** or hot **66** heat exchanges and ambient temperature. To eliminate gravitational convective heat transfer, thermal buffer columns **52, 70** should usually be oriented vertically with the cold end down, as shown in FIGS. **3** and **4**. To eliminate gross shuttle convective heat transfer, the thermal buffer columns **52, 70** should be longer than the peak-to-peak displacement amplitude of the gas within them. To maintain stratified oscillating plug flow in the thermal buffer column, its ends should be provided with flow straighteners (not shown). To eliminate streaming-driven convective heat transfer, thermal buffer columns **52, 70** should be tapered according to U.S. patent application Ser. No. 08/975,766, filed Nov. 21, 1997, incorporated herein by reference.

In another aspect of the present invention, the time-averaged mass flux $\dot{M}$ around the torus (torus **30**, FIG. **3**; torus **60**, FIG. **4**) is controlled to be near zero, to prevent a large steady energy flux $\dot{M}c_p(T_0-T_C)$ from flowing to cold heat exchanger **34** in the refrigerator of FIG. **3** or $\dot{M}c_p(T_H-T_0)$ flowing from hot heat exchanger **66** in the engine of FIG. **4**. In traditional Stirling engines and refrigerators, $\dot{M}$ is exactly zero; otherwise, mass would accumulate steadily on one or the other end of the system. Gedeon, supra, discusses how nonzero $\dot{M}$ can arise in Stirling and pulse-tube cryocoolers whenever a closed-loop path exists for steady flow. Tori **30** (FIG. **3**) and **60** (FIG. **4**) clearly provide such a path; hence, the present invention minimizes $\dot{M}$.

To understand $\dot{M}$, extend the complex notation introduced in Equation (1) to second order, by writing time-dependent variables as

$$\xi(x,t)=\xi_m(x)+Re[\xi_1(x)e^{i\omega t}]+\xi_2(x) \quad (8)$$

The new time-independent term, with subscript "2", is of great interest here.

Gedeon, supra, shows that the second-order time-average mass flux

$$\dot{M}_2=\tfrac{1}{2}Re[\rho_1\tilde{U}_1]+\rho_m U_2 \quad (9)$$

is of primary concern. In acoustics, such second-order mass flux is known as streaming. Gedeon, supra, further shows that $\frac{1}{2}Re[\rho_1\tilde{U}_1]=\rho_m\dot{W}_2|p_m$ in a regenerator, where $\dot{W}_2=\frac{1}{2}Re[p_1\tilde{U}_1]$ is the acoustic power passing through the regenerator. Hence, $\frac{1}{2}Re[\rho_1\tilde{U}_1]$ must be nonzero, and efficient regenerator operation requires that $U_2=-\frac{1}{2}Re[\rho_1\tilde{U}_1]/\rho_m=-\dot{W}_2/p_m$. The consequences of ignoring this requirement can be severe. If $\dot{M}_2\neq 0$, an undesired, streaming-induced heat current

$$\dot{Q}_{loss}\sim\dot{M}_2c_p(T_0-T_C), \text{ refrigerator} \quad (11)$$

$$\sim\dot{M}_2c_p(T_H-T_0), \text{ engine} \quad (12)$$

flows through the system. (This heat can flow through either regenerators **32, 62** or thermal buffer columns **52, 70** in FIGS. **3** and **4**, depending on the sign of $\dot{M}_2$, with equally harmful effect.) For $U_2=0$, the ratio of $\dot{Q}_{loss}$ to the ordinary regenerator loss $\dot{H}_{reg}$ in the refrigerator is of the order of

$$\frac{\dot{Q}_{loss}}{\dot{H}_{reg}} \sim \frac{\gamma}{\gamma-1}\frac{(T_0-T_C)}{T_0}\frac{\dot{W}_C}{\dot{H}_{reg}} \sim \frac{\gamma}{\gamma-1}\frac{(T_0-T_C)}{T_C}\frac{\dot{Q}_C}{\dot{H}_{reg}}. \quad (13)$$

In the third expression, each of the three fractions is >1 for cryocoolers; hence their product is >>1 and the unmitigated streaming-induced heat load would be much greater than the ordinary regenerator loss in a cryocooler.

A laboratory version that embodies the present invention in a refrigerator is shown in FIG. **6**, which is topologically identical to that of FIG. **3**. Refrigerator **80** was filled with 2.4 MPa argon and operated at 23 Hz, so that the acoustic wavelength was 14 m. Refrigerator **80** was driven by an intrinsically irreversible thermoacoustic engine **78**. The dash-dot lines show local axes of cylindrical symmetry. Acoustic power **114** circulates clockwise through inertance **82**, compliance **84**, and refrigerator parts **86** of the apparatus. Heavy flanges **102, 92** around first ambient heat exchanger **88** and second ambient heat exchanger **96** contain water jackets. O-rings, most flanges, and bolts are omitted for clarity.

Note that second ambient heat exchanger **96** is not necessary for the operation of the invention. It does provide some flow straightening for the ambient end of thermal buffer column **104**. Water passages were included in second ambient exchanger **96** because the parts were being reused from unrelated tests involving a traditional OPTR configuration.

The heart of refrigerator **86**, regenerator **98**, was made of a 2.1 cm thick stack of 400-mesh (i.e., 400 wires per inch) twilled-weave stainless-steel screens punched at 6.1 cm diameter. The total weight of the screens in the regenerator was 170 gm. The calculated value of the hydraulic radius of this regenerator was approximately 12 μm, based on its geometry and weight. The hydraulic radius is much smaller than the thermal penetration depth of the argon (100 ρm at 300 K), as required of a good regenerator. The stainless-steel pressure vessel **94** around regenerator **98** had a wall thickness of 1.4 mm. Thermal buffer column **104** was a simple open cylinder, 3.0 cm id and 10.3 cm long, with 0.8 mm wall thickness. The diameter of buffer column **104** is much greater than the viscous penetration depth of the argon (90 μm at 300 K), and its length is greater than the 1-cm gas displacement amplitude in it at a typical operating point near $|p_1|/p_m \approx 0.1$. At each end, a few 35-mesh copper screens (not shown) served as simple flow straighteners to help maintain oscillatory plug flow in thermal buffer column **104**. The high density of argon enhances the gravitational stability of this plug flow, so that careful flow straightening and tapering were not embodied in this initial laboratory refrigerator. However, a gas providing more power density, such as helium, may be used instead of argon, and the apparatus would be likely to need careful flow straightening and tapering for maximum performance. To obtain gravitational stability, the orientation of the refrigerator assembly was vertical, as shown in FIG. **6**.

For test purposes, cold heat exchanger **106** between regenerator **98** and thermal buffer column **104** was a 1.8Ω length of NiCr ribbon wound zigzag on a fiberglass frame. Wires from the heater and a thermometer passed axially along the thermal buffer column to leak-tight electrical feedthroughs at room temperature. The two water-cooled heat exchangers (first ambient heat exchanger **88** and second ambient heat exchanger **96**) were of shell-and-tube construction, with the Reynolds number of order 10^4 at $|p_1|/p_m \approx 0.1$ in the argon inside the 1.7-mm-diameter, 18-mm long tubes. First ambient heat exchanger **88** had **365** such tubes, and second ambient heat exchanger **96** had **91**.

Inertance **82** was a simple metal tube with 2.2 cm id and 21 cm length, with 7° cones, as shown in FIG. **6**, at both ends to reduce turbulent end effects. Inertance **82** and refrigerator **86** components were sealed into flat plates above and below by rubber O-rings to enable easy modifications. The flat plates were held at a fixed separation by flange extensions and a cage of stout tubes (not shown) through which long bolts passed. Compliance **84** was half an ellipsoid with 2:2:1 aspect ratio, with a volume of 950 cm^3.

Refrigerator **86** was configured first as shown in FIG. **6**, but without flexible diaphragm **108** (which may be a balloon-type diaphragm, or the like) installed. At $|p_{1C}|/p_m = 0.068$ the refrigerator did not cool below 19° C., essentially the temperature of the cooling water supplied to the water-cooled heat exchangers that day. However, the pressure phasors were close to predictions and the refrigerator's cold temperature was very strongly independent of heat load applied to the cold heat exchanger, e.g., at $|p_{1C}|/p_m = 0.07$, an applied load of 70 W raised T_C to only 35° C., as shown by the half-filled circles in FIG. **7**. Hence, the acoustic phenomena and gross cooling power were substantially as expected, and an extremely large nonzero $\dot{M}$ was effectively keeping cold heat exchanger **106** thermally anchored to ambient heat exchanger **88**, overwhelming the otherwise satisfactory cooling power.

To show that the initial refrigerator performance shown as half-filled circles in FIG. **7** was due to nonzero mass flux, flexible diaphragm **108** was installed above second ambient heat exchanger **96**, as shown in FIG. **6**. Flexible diaphragm **108** was selected to be acoustically transparent while blocking $\dot{M}$ completely. With flexible diaphragm **108** in place, refrigerator **86** performed well, confirming that maintaining $\dot{M}=0$ results in successful operation of this type of Stirling refrigerator. Flexible diaphragm **108** was operated at $|p_{10}|/p_m$ ranging from 0.04 to 0.10. In one set of measurements, $|p_{1C}|/p_m = 0.054$ was maintained, while varying T_C from −115° C. to 7° C. by adjusting an electric heater power $\dot{Q}$Cat cold heat exchanger **106**. (T_0=13° C. throughout.) The filled symbols and lines in FIG. **7** are the resulting measurements and calculations, respectively. The experimental points show the electric heater power $\dot{Q}_C$ applied to cold heat exchanger **106** to maintain a given T_C and the line is the corresponding calculation. Experimental points also show measured acoustic power $\dot{W}_{sidebranch}$ delivered from the side branch, and the long-dash line is the corresponding calculation. The short-dash line shows calculated values of recovered power (i.e., the acoustic power passing through flexible diaphragm **108**).

The data depicted in FIG. **7** show that the cooling power drops and the acoustic power supplied from the side branch rises as T_C decreases. The calculations, which are in reasonable agreement with the experiments, provide insight to the main causes of these trends. First, the calculated gross cooling power $\dot{W}_C = \frac{1}{2}\mathrm{Re}[p_{1C}\tilde{U}_{1C}]$ is nearly constant at 40 W, independent of T_C for these measurements. As discussed near Equation (2), under the most ideal circumstances this would be the cooling power. The decrease in calculated $\dot{Q}_C$ below 40 W as T_C decreases is nearly proportional to T_0-T_C and is almost entirely due to heat flux through regenerator **98**. The difference between measured and calculated $\dot{Q}_C$ is also proportional to T_0-T_C, rising to 10 W at T_C=−120° C. This could easily be due to a combination of ordinary heat leak through the insulation and streaming- or jet-driven convection in thermal buffer column **104**. Second, under the most ideal circumstances—with 40 W of cooling power and

with Carnot efficiency $\dot{Q}_C/\dot{W}=T_C/(T_0-T_C)$—the required net acoustic power would be $\dot{W}=(40 \text{ watts})(T_0-T_C)/T_C$ which rises from zero at $T_C=T_0$ to 35 W at $T_C=-120°$ C. This accounts for most of the 40 W rise in calculated $\dot{W}_{sidebranch}$ with falling T_C in FIG. 7. The measurements of $\dot{W}_{sidebranch}$ exceed calculations by roughly 30%, for unknown reasons. Calculations show that approximately 5 W of acoustic power is dissipated in second ambient heat exchanger **96** under flexible barrier **108**, 15 W is lost due to viscosity in regenerator **98** and adjacent heat exchangers **88**, **106**, and 10 W is dissipated in inertance **82**.

If this were a traditional orifice pulse tube refrigerator, $\dot{W}_C$=40 W would be dissipated in an orifice. In FIG. **7**, the calculated fedback acoustic power $\dot{W}_{recovered}$, which is one aspect of this invention, is near 30 W; hence, approximately 75% of $\dot{W}_C$ is recovered and fed back into the resonator through side branch **112**. Note that at the highest temperatures $\dot{W}_{recovered}$ is comparable to $\dot{W}_{sidebranch}$. In other words, at these temperatures the toroidal configuration reduces the acoustic power delivered from intrinsically irreversible thermoacoustic engine **78** to refrigerator **80** to roughly half of what it would be in a traditional orifice pulse tube refrigerator.

To demonstrate an engine embodiment of this invention, engine **120** shown in FIG. **8** was constructed. It was filled with 3.1 MPa helium and operated at 70 Hz, with a corresponding acoustic wavelength of 14 m. The small circles in and below regenerator **122** indicate the location of some temperature sensors. Pressure sensors were also provided to measure P_{10} and P_{1H}. Most external hardware is shown in the figure, except for a cage of heavy bolts surrounding the sliding joints **148**, the acoustic resonator, and a variable acoustic load.

Regenerator **122** was made from a 7.3 cm stack of 120 mesh stainless steel screen machined to a diameter of 8.89 cm. The stack of screens was contained within a thin wall stainless steel can for ease of installation and removal. Based on the total weight of screen in the regenerator, the volume porosity was 0.72 and the hydraulic radius was about 42 μm. This is smaller than the thermal penetration depth of helium, which varies from 140 μm to 460 μm through regenerator **122**. The stainless steel pressure vessel **124** around regenerator **122** had a wall thickness of 12.7 mm at the hot end and was tapered to a thickness of 6.0 mm at the cold end.

Thermal buffer column **126** was an open cylinder having the same inner diameter as regenerator **122** and was 26.4 cm long. Its inner diameter was much larger than the viscous and thermal penetration depths of the helium, and its length was much greater than the gas displacement (2.5 cm) at a typical operating point of $|p_1|/p_m$=0.05. The wall thickness was initially 12.7 mm at the hot end and was stepped down to 6.0 mm at a distance of 9.6 cm from the hot end. No effort was made to taper the thermal buffer column to suppress boundary-layer driven streaming within the column (see U.S. patent application Ser. No. 08/975,766). Operating data indicated that this form of streaming was present and was carrying several 100 Watts of heat. These measurements show the need for tapering the thermal buffer column in this type of engine. The small taper angle θ (a few degrees) shown to reduce streaming in the '766 application would not be readily apparent from FIG. **8**. Thus, FIG. **8** should also be considered to include a tapered embodiment of thermal buffer column **126**. It will be appreciated from the '766 application that the amount and direction of the taper that suppresses streaming is not intuitively apparent and must be determined from the particular embodiment and operating conditions of thermal buffer column **126**.

For test purposes, hot heat exchanger **128** consisted of an electrically heated Ni—Cr ribbon wound zigzag on an alumina frame. Electrical leads for hot heat exchanger **128** entered thermal buffer column **126** at its ambient temperature end and passed axially up the column to the ribbon. Power flowing into hot heat exchanger **128** was measured using a commercial wattmeter.

First ambient heat exchanger **132** and second ambient heat exchanger **134** were water cooled heat exchangers of shell-and-tube construction. First ambient heat exchanger **132** contained 299 2.5 mm id, 20 mm long tubes. A typical Reynolds number in the tubes was 3,000 at $|p_1|/p_m$=0.05. Second ambient heat exchanger **134** contained 109 4.6 mm id, 10 mm long tubes. A typical Reynolds number in the tubes was 16,000 at $|p_1|/p_m$=0.05. Second ambient heat exchanger **134** was included for test purposes and would not be needed for actual use of the engine.

The main part of inertance **136** was made from commercial, schedule **40**, 2.5" nominal, carbon steel pipe. Light machining was performed on the inside surface to improve the finish. To reconnect inertance **136** to the main section of the engine, a standard 2.5" pipe cross **138** and a standard 4" to 2.5" reducing tee **192** were used. The total length of inertance **136** was 59 cm, and the inside diameter was approximately 6.3 cm. Compliance **144** consisted of two commercial, 4" nominal, 90°, short radius elbows. The total volume of compliance **144** was 0.0028 m^3. A commercial 4" to 2.5" reducer **146** was used to smoothly adapt inertance **136** to compliance **144**. Inertance **136** included sliding joints **148** to allow inertance **136** to lengthen as thermal buffer column **126** and pressure vessel **124** thermally expanded.

In the engine embodiment shown in FIG. **8**, $\dot{M}_2$ was suppressed using a hydrodynamic approach, e.g., jet pump **140**, discussed below. First, baselines were established for comparison. Engine **120** was run with no attempt made to block $\dot{M}_2$. Engine **120** was then operated with rubber diaphragm **152** installed at the junction between reducer **146** and compliance **144**. In both of the runs, the pressure phasors p_{10} and p_{1H} were close to the estimates based on prior calculations. The majority of the difference between these two runs is the presence of $\dot{M}_2$.

FIG. **9** shows the temperature distributions in regenerator **122** in these two runs. In both runs, increasing amounts of heat were applied to hot heat exchanger **128** until the pressure amplitude reached $|p_{10}|/p_m$=0.05. The only load on the engine was the acoustic resonator itself (not shown). Therefore, T_H should be nearly the same for both cases. With the diaphragm in place, the temperature rises linearly from the ambient end to the hot end. With no $\dot{M}_2$, this linear dependence is expected because the thermal conductivity of helium and stainless steel depend only weakly on temperature.

The temperature distribution with diaphragm **152** removed and $\dot{M}_2$ not restricted is greatly different. Equation 9 and the subsequent discussion show that $\dot{M}_2$ flows in the same direction as the flow of acoustic power. In this case $\dot{M}_2$ enters regenerator **122** from first ambient heat exchanger **132**. As seen in FIG. **9**, this flux of cold gas reduces the temperature of regenerator **122** for nearly its entire length. The temperature rises quickly near the hot end due to the presence of hot heat exchanger **128**. Note that, in FIG. **9**, the lines are only guides to the eye, and do not reflect the actual temperatures between the data points. The temperature near 7.2 cm can be assumed to be nearly the same as that at 10 cm. For a rough estimate of $\dot{M}_2$, compare the amounts of

heat input, $\dot{Q}_H$, needed to run the engine at this pressure amplitude with and without diaphragm **152**. With diaphragm **152** in place, $\dot{Q}_H$=1250 W. Without diaphragm **152**, $\dot{Q}_H$=2660 W. This difference in heat input, $\Delta\dot{Q}_H$, should be given by

$$\Delta\dot{Q}_H=\dot{M}_2 c_p(T_H-T_0) \tag{14}$$

Using Equation (14), $\dot{M}_2$=1.5×10^{-3} kg/s.

One way to suppress $\dot{M}_2$ is to impose a time averaged pressure drop, Δp_2 across regenerator **122** that would drive an equal but oppositely directed amount of $\dot{M}_2$ through regenerator **122**. The required Δp_2 can be estimated using the low-Reynolds-number limit of FIG. **7–9** of Kays and London, *Compact Heat Exchangers,* (McGraw-Hill, NY 1964), incorporated herein by reference,

$$\frac{dp_2}{dx}\cong\frac{6\dot{M}_2\mu}{\rho_m S r_h^2} \tag{15}$$

for the pressure gradient in a screen bed of cross-sectional area S and hydraulic radius r_h, where μ is the viscosity. The numerical factor depends weakly on the volumetric porosity of the bed. For the data shown in FIG. **9** and the estimate of $\dot{M}_2$, the required pressure drop is 370 Pa.

An alternate way to estimate $\dot{M}_2$ within regenerator **122** is to use Equation (9) and the subsequent discussion, i.e., $\dot{M}_2=\rho_m\dot{W}_2/p_m$. Under the conditions of the experiment, at the ambient end of regenerator **122**, $\dot{W}_2$ is calculated to be $\dot{W}_2$=850 W giving $\dot{M}_2$=1.3×10^{-3} kg/s. The experimental estimate of $\dot{M}_2$ and the calculation are in rough agreement, suggesting that the estimate of Δp_2~370 Pa is approximately correct.

In the limit of low viscosity or large tube diameters and in the absence of turbulence, p_2 would be described by some acoustic version of the Bernoulli equation. This suggests that an acoustically ideal path connecting the two ends of the regenerator would impose across regenerator **122** a pressure difference of the order of $\Delta[\rho_m u_1\tilde{u}_1]$ where u_1 is the complex velocity amplitude. (Such an ideal path might include a thermal buffer column, inertance, and compliance, without heat exchangers or other components having small passages.) This pressure difference is typically much smaller than the Δp_2 that is required for $\dot{M}_2$=0. Hence, to produce the required Δp_2 an additional physical effect or structure in the path is needed, relying on turbulence, viscosity, or some other physical phenomenon not included in the Bernoulli equation.

Asymmetry in hydrodynamic end effects can produce this required Δp_2. In a tapered transition between a small-diameter tube, where $|u_1|$ is large, and a large-diameter tube, where $|u_1|$ is small, turbulence would be avoided and Bernoulli's equation would hold if the taper were sufficiently gentle. At the opposite extreme, for an abrupt transition, a large $|u_1|$ generates significant turbulence, and further the oscillatory pressure drop across an abrupt transition should reflect the phenomena known as "minor losses" in high-Reynolds-number steady flow. If the gas displacement amplitude is much greater than the tube diameter, the flow at any instant of time has little memory of its past history, so that the acoustic behavior can be deduced from careful time integration of the well-known expressions for the steady-flow phenomena.

In steady flow through an abrupt transition, the minor loss-induced deviation Δp_{ml} of the pressure from the Bernoulli equation ideal is given by

$$\Delta p_{ml}=K\tfrac{1}{2}\rho u^2 \tag{16}$$

where K is the minor-loss coefficient, which is well known for many transition geometries, and u is the velocity. K depends strongly on the direction of flow through the transition. In the example shown in FIGS. **10A** and **10B**, a small flanged tube **160** is connected to an essentially infinite open space **164**. When a gas **164** (at velocity u inside tube **162**) flows out of the tube **162**, a jet occurs, and kinetic energy is lost to turbulence **166** downstream of the jet; K_{out}=1. In contrast, when gas flows into tube **162**, as shown in FIG. **10B**, streamlines **168** in open space **164** are widely and smoothly dispersed; K is between 0.5 and 0.04, with smaller values for larger radius r of rounding of the edge of the entrance.

If $u_1=|u_1|\sin\omega t$, the time-averaged pressure drop is obtained by integrating Equation (16) in time:

$$\overline{\Delta p_{ml}}= \tag{17}$$
$$\frac{\omega}{2\pi}\left(\int_0^{\pi/\omega}K_{out}\frac{1}{2}\rho|u_1|^2\sin^2\omega t\,dt-\int_{\pi/\omega}^{2\pi/\omega}K_{in}\frac{1}{2}\rho|u_1|^2\sin^2\omega t\,dt\right)=$$
$$\frac{1}{8}\rho|u_1|^2(K_{out}-K_{in})$$

This hydrodynamic mean pressure difference can be used as the source of Δp_2 across the regenerator necessary to force $\dot{M}_2$=0. Such simple control of $\dot{M}_2$ is not without penalty, however; acoustic power is dissipated at a rate

$$E=S\frac{\omega}{2\pi}\int_0^{2\pi/\omega}\Delta p_{ml}u\,dt= \tag{18}$$
$$S\frac{\omega}{2\pi}\left(\int_0^{\pi/\omega}K_{out}\frac{1}{2}\rho|u_1|^3\sin\omega t\,dt-\int_{\pi/\omega}^{2\pi/\omega}K_{in}\frac{1}{2}\rho|u_1|^3\sin^3\omega t\,dt\right)=$$
$$\frac{1}{3\pi}\rho|u_1|^2|U_1|(K_{out}+K_{in})$$
$$=\frac{8}{3\pi}\overline{\Delta p_{ml}}|U_1|\frac{K_{out}+K_{in}}{K_{out}-K_{in}} \tag{19}$$

where S is the area of the small tube **162**. Equation (19) shows that the best way to produce a desired $\overline{\Delta p_{ml}}$ is to insert the hydrodynamic mass-flux suppressor at a location where $|U_1|$ is small, and to shape it so that $K_{out}-K_{in}$ is as large as possible.

In engine **120** (FIG. **8**), $|U_1|$ is smallest adjacent to regenerator **122**, but that was an inconvenient location for adding an additional component. Second ambient-temperature heat exchanger **134** has only slightly larger $|U_1|$ and already requires some extra dissipation to ensure that p_{10} leads p_{1H} slightly, so the space below second ambient temperature heat exchanger **134** was chosen as the location for experiments on hydrodynamic mass-flux suppression. In this embodiment, hydrodynamic mass-flux suppressor **140** was a "jet pump", formed from a brass block bored through with 25 identical tapered holes, each 1.82 cm long, 8.05 mm diameter at the upper end nearest second ambient temperature heat exchanger **134** and 5.72 mm diameter at the lower end. End effects at the well-rounded small ends of the holes are strongly asymmetric, causing the desired $\overline{\Delta p_{ml}}$, while the velocities at the large ends of the holes are small enough that minor losses are negligible. The tapers joining the ends are gradual enough to prevent minor losses in-between. For the

chosen geometry, jet pump **140** was estimated to create a pressure of Δp_2=930 Pa. However, this estimate is based on a calculation that assumes no interaction between the minor losses at the two ends of jet pump **140**. For steady flow, it is known that two minor loss sites located close together result in less Δp_2 than the sum of the individual Δp_2's.

Jet pump **140** was installed and engine **120** was run at the same operating point as the two other sets of data in FIG. **9**. The temperature distribution with jet pump **140** was nearly restored to the distribution with rubber diaphragm **152**. Also, the amount of heat input needed to reach this operating point with rubber diaphragm **152** was only Q_H=1520 W. The additional heat required without the rubber diaphragm **152** was 1400 Watts. The use of jet pump **140** reduced this by 82% to 260 Watts. This clearly demonstrates the effectiveness of jet pump **140**.

By using a variable acoustic load (not shown) to increase the acoustic load on the engine, measurements of the temperature distribution were made as a function of T_H at a fixed value of $|p_{10}|/p_m$=0.05. These measurements showed no detectable change in the linearity of the temperature distribution for $200° \leqq T_H \leqq 725°$ C. Therefore, jet pump **140** appeared to be very immune to variations in the load conditions. Finally, by varying $\dot{Q}_H$ at fixed acoustic load, measurements were made of the temperature distribution as function of p_1 at fixed T_H~525° C. The temperature distribution did not change in the range $0.03 \leqq |p_{10}|/p_m \leqq 0.05$. At higher pressure amplitudes, the jet pump weakened relative to other sources of Δp_2. At the highest pressure amplitude achieved, $|p_{10}|/p_m$=0.075, the temperature in the middle of the regenerator dropped from its low amplitude value of 310° C. to 235° C. This amounts to only a 15% change relative to $T_H - T_0$~500° C.

The efficiencies obtained during these measurements with jet pump **140** are shown in FIGS. **11A** and **11B**. During these measurements, the highest efficiency $\eta = \dot{W}/Q_H$=0.17, and the highest fraction of Carnot efficiency, $\eta_{II} = \eta/\eta_C$=0.27, where the Carnot efficiency is $\eta_C = 1 - T_0/T_H$. With rubber diaphragm **152** in place, the highest observed values were η=0.21 and η_{II}=0.32. In measuring the work output of the engine, $\dot{W}$, only the acoustic power delivered to the variable acoustic load was counted; the resonator dissipation was not included. Hence, these efficiencies represent the engine plus resonator; the efficiencies with which the engine delivered power to the resonator are even higher.

It may sometimes be desirable to adjust the strength of the hydrodynamic method for mass-flux suppression while a traveling-wave device is operating in order to provide whatever Δp_2 is needed to enforce $\dot{M}_2$=0 over a broad range of operating conditions. To test such a variable hydrodynamic method, the refrigerator apparatus shown in FIG. **6** was modified to include a slit jet pump as shown in FIGS. **12A** and **12B** in place of flexible diaphragm **108** shown in FIG. **6**. Slit **172** provides asymmetric flow as illustrated in FIGS. **10A** and **10B**, and hence provides Δp_2 as shown in Equation (17) with K_{out}~1 and K_{in}~0.1. Pivot point **174** allows right wall **176** of slit **172** to be moved, e.g., by a lever (not shown) connected through a pressure seal to an external knob for manual adjustment or by an automatic controller that is regulated by, e.g., a temperature sensor in the middle of regenerator **98** (FIG. **6**). Moving right wall **176** of slit **172** in this way adjusted the area of slit **172**, and hence changed $|u_1|$ relative to $|U_1|$ so that Δp_2 was changed according to Equation (17).

Tests with this setup over a range of T_C (from 0° to −70° C.) and a range of pressure amplitudes $|p_1|/p_m$ (from 0.03 to 0.05) showed that the width of slit **172** could be adjusted to keep the temperature in the middle of regenerator **98** approximately equal to the average of T_C and T_0, indicative of $\dot{M}_2$=0. Under these circumstances, the performance of the refrigerator was similar to its performance when flexible diaphragm **108** was used.

The above description of the invention is mostly in terms of a refrigerator with a sub-wavelength torus and with a flexible-barrier method of mass-flux suppression and in terms of an engine with a sub-wavelength torus and with a hydrodynamic method of mass-flux suppression. However, the use of a thermal buffer column and either method of mass-flux suppression is applicable to both engines and refrigerators, whether these engines and refrigerators employ sub-wavelength tori as described herein or more nearly full-wavelength tori as described by Ceperley. It should also be apparent from the description that additional flexible-barrier methods (including bellows) and additional hydrodynamic methods (including the adjustable method discussed above) are also useful. Although mass-flux suppression is described herein as localized, it could be distributed throughout several regions of the apparatus, such as by employing tapered passages in one or more heat exchangers and using asymmetric hydrodynamic effects at the "tee" joining the torus and the side branch (see, e.g., FIG. **8**).

It should also be apparent that all aspects of the present invention are as applicable to heat pumps as to refrigerators, that an engine and refrigerator can share the same torus, that multiple devices can share a torus, and that multiple tori can be connected in many ways, such as by sharing a common inertance and a common compliance. In such situations, each torus may require its own mass-flux suppressor, and each heat exchanger at a temperature other than ambient temperature may benefit from an adjacent thermal buffer column.

FIGS. **13A–D** illustrate some of these embodiments. In the description of these figures, the terms regenerator, heat exchanger, mass-flux suppressor, thermal buffer, inertance, compliance, and other terms have the same meaning as with the above detailed descriptions and will not be described in detail. It is the arrangement of these components that provides the different embodiments and not the function of the components.

Referring first to FIG. **13A**, there is shown a heat pump configuration of components. Torus **180** defines inertance **202** and compliance **198**. Regenerator **182** is located in torus **180** with an ambient heat exchanger **184** downstream from regenerator **182** relative to the circulating acoustic power. Hot heat exchanger **186** is adjacent to and upstream of regenerator **182**. Mass flux suppressor **185** is shown downstream from ambient heat exchanger **184** but may be located an any convenient location in torus **180**. In this instance, thermal buffer column **188** is located adjacent hot heat exchanger **186**, which is the heat exchanger that defines the operating temperature of the device. Acoustic power **192** is generated by acoustic device **196** and input to torus **180** through side branch **194**.

FIG. **13B** depicts a combination of an acoustic source **40** formed by an engine according to the present invention as described in FIG. **4** and an acoustic sink **76** formed by a refrigerator according to the present invention as described in FIG. **3**, where like numbers represent like components that can be identified by reference to FIGS. **3** and **4**. A common side branch corresponds to side branches **44** and **74** with acoustic power flow **42**, **72** as shown in FIGS. **3** and **4**.

FIG. **13C** is a further refinement of the embodiment shown in FIG. **13B** where engine **212** and refrigerator **230** are incorporated into a single torus **210**. Engine **212** includes

regenerator **216**, with adjacent heat exchangers **214** (ambient temperature) and **218** (operating temperature), with operating temperature heat exchanger **218** downstream from regenerator **216** and adjacent thermal buffer column **222** downstream from operating temperature heat exchanger **218**. If needed, engine **212** may have associated inertance **224** and compliance **226** to provide suitable phasing of the output acoustic power.

Refrigerator **230** receives the acoustic power output from engine **212** and includes regenerator **234** with adjacent heat exchangers **232** (ambient temperature) and **236** (operating temperature). Thermal buffer column **238** is downstream from operating temperature heat exchanger **236**. If needed, additional inertance **242** and compliance **244** may be defined by torus **210**. In accordance with the present invention, mass-flux suppressor **240** is included in torus **210**. Suppressor **240** may be generally located anywhere within torus **210** and may be lumped at one location or provided as a distributed suppressor or discrete multiple components within torus **210**.

FIG. **13D** schematically depicts a parallel configuration of multiples of the refrigerator shown in FIG. **3**. Identical components are described with the same reference numbers or primed reference numbers and are individually discussed with reference to FIG. **3**. As shown, one or more refrigerator sections may be joined by a common column **50** for the circulating acoustic power **38**, **38'**. Column **50** may be configured to define a common inertance for the parallel refrigerators. It will be understood that more than two refrigerators may be connected in parallel. Also, while FIG. **13D** depicts refrigerators, the same configuration could be used for the engine shown in FIG. **4**.

The foregoing description of Stirling cycle traveling-wave refrigerators and engines has been presented for purposes of illustration and description and is not intended to be exhaustive or to limit the invention to the precise form disclosed, and obviously many modifications and variations are possible in light of the above teaching. The embodiments were chosen and described in order to best explain the principles of the invention and its practical application to thereby enable others skilled in the art to best utilize the invention in various embodiments and with various modifications as are suited to the particular use contemplated. It is intended that the scope of the invention be defined by the claims appended hereto.

What is claimed is:

1. A pistonless traveling-wave device having

a. a torus for circulating acoustic energy in a direction through a fluid;

b. a regenerator located in the torus;

c. a first heat exchanger located on a downstream side of the regenerator relative to the direction of the circulating acoustic energy; and

d. a second heat exchanger located on an upstream side of the regenerator;

wherein the improvement comprises:

e. a mass-flux suppressor located in the torus to minimize time averaged mass flux of the fluid.

2. A pistonless traveling-wave device according to claim **1**, further including:

f. a thermal buffer column located in the torus adjacent the one of the first or second heat exchangers that is at an operating temperature of the traveling-wave device to thermally isolate that heat exchanger.

3. A pistonless traveling-wave device according to either one of claims **1** or **2**, wherein the torus is shorter than a wavelength of the circulating acoustic energy.

4. A pistonless traveling-wave device according to claim **3**, wherein the torus defines acoustic inertance and acoustic compliance portions.

5. A pistonless traveling-wave device according to claim **2**, wherein the thermal buffer column has a diameter much greater than a viscous penetration depth of the fluid.

6. A pistonless traveling-wave device according to claim **2**, wherein the thermal buffer column has a length greater than a peak-to-peak fluid displacement amplitude.

7. A pistonless traveling-wave device according to any one of claims **5** or **6**, wherein the thermal buffer column is tapered.

8. A pistonless traveling-wave device according to any one of claims **1** or **2**, wherein the mass-flux suppressor is a flexible diaphragm.

9. A pistonless traveling-wave device according to any one of claims **1** or **2**, wherein the mass-flux suppressor is a hydrodynamic jet pump having a geometry effective to provide asymmetric end effects to generate a pressure drop to oppose mass flux through the jet pump.

10. A pistonless traveling-wave device according to any one of claims **1** or **2**, wherein the device is a refrigerator and the downstream heat exchanger is a cold heat exchanger.

11. A pistonless traveling-wave device according to claim **10**, wherein the torus is shorter than a wavelength of the circulating acoustic energy.

12. A pistonless traveling-wave device according to claim **11**, where the torus defines acoustic inertance and acoustic compliance portions.

13. A pistonless traveling-wave device according to any one of claims **1** or **2**, wherein the device is an engine and the downstream heat exchanger is a hot heat exchanger.

14. A pistonless traveling-wave device according to claim **13**, wherein the torus is shorter than a wavelength of the circulating acoustic energy.

15. A pistonless traveling-wave device according to claim **14**, wherein the torus defines acoustic inertance and acoustic compliance portions.

16. A pistonless traveling-wave device according to any one of claims **1** or **2**, wherein the device is a heat pump and the upstream heat exchanger is a hot heat exchanger.

17. A pistonless traveling-wave device according to claim **16**, wherein the torus is shorter than a wavelength of the circulating acoustic energy.

18. A pistonless traveling-wave device according to claim **17**, wherein the torus defines acoustic inertance and acoustic compliance portions.

19. A pistonless traveling-wave device according to claim **10**, further including an engine for generating the acoustic energy having a second regenerator, a hot heat exchanger downstream of the second regenerator relative to a direction for propagating the acoustic energy and an ambient heat exchanger upstream of the second regenerator.

20. A pistonless traveling-wave device according to claim **19**, wherein the engine is located in a second torus connected to the torus with the refrigerator and the second torus includes a second mass-flux suppressor.

21. A pistonless traveling-wave device according to claim **19**, wherein the engine is located in the torus with the refrigerator.

22. A pistonless traveling-wave device according to claim **10**, further including at least a second refrigerator in a second torus, where the second torus has at least a portion of the volume in common with the torus to form a parallel connection of the refrigerator and the second refrigerator.

* * * * *